Environmental and hydrologic controls on sediment and organic carbon export from a subalpine catchment: insights from a time-series

Melissa S. Schwab[1,2], Hannah Gies[1], Chantal V. Freymond[1,3], Maarten Lupker[1,4], Negar Haghipour[1,5], Timothy I. Eglinton[1]

[1]Department of Earth Sciences, ETH Zurich, Zurich, 8092, Switzerland
[2]Now at Jet Propulsion Laboratory, California Institute of Technology, Pasadena, 91109, USA
[3]Now at Gruner, Basel, 4020, Switzerland
[4]Now independent, Bern, 3014, Switzerland
[5]Laboratory of Ion Beam Physics, ETH Zurich, Zurich, 8093, Switzerland

Correspondence to: Melissa S. Schwab (melissa.s.schwab@jpl.nasa.gov)

Abstract. Studies engaging in tracking headwater carbon signatures downstream remain sparse, despite their importance for constraining transfer and transformation pathways of organic carbon (OC) and developing regional-scale perspectives on mechanisms influencing the balance between remineralization and carbon export. Based on a 40-month time series, we investigate the dependence of hydrology and seasonality on the discharge of sediment and OC in a small (350 km^2) Swiss subalpine watershed (Sihl River basin). We analyze concentrations and isotopic compositions ($\delta^{13}C$, $F^{14}C$) of particulate OC and use dual-isotope mixing and machine learning frameworks to characterize and estimate source contributions, transport pathways, and export fluxes. The majority of transferred OC is sourced from plant biomass and soil material. The relative amount of bedrock-derived (petrogenic) OC, abundant in headwater streams, progressively decreases downstream in response to a lack of source material and efficient overprinting with biospheric OC, illustrating rapid organic matter alteration over short distances. Large variations in OC isotopic compositions observed during baseflow conditions converge and form a homogenous mixture enriched in OC and characterized by higher POC- $F^{14}C$ values following precipitation-driven events. Particulate OC isotopic data and model results suggest that storms facilitate surface runoff and the inundation of riparian zones, resulting in the entrainment of loose plant-derived debris and surficial soil material. Although particle transport in the Sihl River basin is mainly driven by hydrology, subtle changes in bedrock erosivity, slope angle, and floodplain extent likely have profound effects on the POC composition, age, and export yields.

1 Introduction

River networks serve as an aquatic continuum, ultimately connecting the terrestrial with the marine biosphere (Aufdenkampe et al., 2011). Disproportional to their spatial extent, water bodies are active sites for transport, transformation, and storage of significant portions of organic carbon (OC) mobilized from the terrestrial environment (Battin et al., 2009). Annually, between 1.90 and 2.95 PgC yr^{-1} are entrained into inland waters (Cole et al., 2007; Tranvik et al., 2009; Regnier et al., 2022).

The majority of this carbon is lost during transfer due either to remineralization and outgassing or to burial in lakes and floodplains. Ultimately, only 0.80-0.95 PgC yr^{-1} reach marine coastal regions (Tranvik et al., 2009; Battin et al., 2009; Raymond et al., 2013; Lauerwald et al., 2015; IPCC, 2021; Regnier et al., 2022). However, anthropogenic and climate-driven changes markedly influence erosional processes and thus may perturb the translocation and sequestration of OC in freshwater systems. The human-induced lateral transfer of carbon adds ~0.60 PgC yr^{-1} to inland waters which are largely respired and buried during fluvial transit (Regnier et al., 2022; Lauerwald et al., 2020; Li et al., 2019). The resulting OC flux to marginal shelves deviates by only 0.15 PgC yr^{-1} from pre-industrial values (Regnier et al., 2022).

It is well established that small mountainous rivers deliver substantial quantities of sediment and particulate organic carbon (POC) to the oceans (Milliman and Syvitski, 1992; Lyons et al., 2002; Leithold et al., 2006; Hilton et al., 2012; Goñi et al., 2013). These systems are often characterized by a steep basin morphology, with little to no developed floodplains. The resulting basin storage capacity is insufficient to retain the large amounts of eroded sediments and soils exported from upstream catchments (Wheatcroft et al., 2010; Milliman and Farnsworth, 2013). During storm-driven events, mountainous rivers are strongly coupled to hillslope processes and often provide the main source of sediment to downstream channels (Milliman and Syvitski, 1992; Hilton et al., 2012).

A decrease in the OC content of the suspended load is commonly observed with increasing discharge in high sediment-yield small mountainous rivers (Masiello and Druffel, 2001; Coynel et al., 2005; Leithold et al., 2016). This decline corresponds to the dilution with generally carbon-poor bedrock material, with the proportion of fossil OC concomitantly increasing with rising sediment yields in small river systems as they share a common source and transport pathways (Blair et al., 2003; Komada et al., 2004; Leithold et al., 2006; Hilton et al., 2011a). On the other hand, while deep-seated landslides and gully erosion mobilize predominantly bedrock-sourced (petrogenic) OC, surface runoff and shallow landslides preferentially remove fresh litter and organic-rich surface soils (Hovius et al., 2000; Hilton et al., 2008b; Hatten et al., 2012; Goñi et al., 2013). In headwaters, significant portions of biospheric organic matter are exported in the form of coarse POC (>1 mm) encompassing leaves, needles, and wood fragments (Turowski et al., 2016; Rowland et al., 2017). In contrast to fine-grained OC, which can remain in suspension for prolonged periods, coarse particles are often deposited in headwater valley segments due to gravitational settling or retention in log jams (Wohl et al., 2012; Jochner et al., 2015). Interaction of woody debris and the gravel bedload might lead to grinding and size reduction, ultimately adding to the fine POC pool (Turowski et al., 2016). Despite these mechanisms, restricting the transport of coarse POC, studies showed that event-driven floods can effectively recruit and transfer vascular plant debris as driftwood (West et al., 2011; Wohl and Ogden, 2013; Wohl, 2017; Ruiz-Villanueva et al., 2019) or as a component of the suspended load (Schwab et al., 2022) to continental margins.

Overall, despite the growing recognition of the substantial and rapid downstream transfer of terrestrial OC from headwater streams (Leithold et al., 2016; Wheatcroft et al., 2010; Goñi et al., 2013) and increased understanding of the processes controlling organic matter during its transfer through lowlands and floodplains (e.g., Bouchez et al., 2010; Hemingway et al., 2017; Repasch et al., 2021), river segments that connect small, mountainous streams with lowland systems remain

underexplored. A few studies address temporal dynamics of POC export in moderately steep river basins spanning timescales of individual storm events to intra- and inter-annual variability (Smith et al., 2013; Hatten et al., 2012). Even fewer studies examine the downstream evolution, composition, and molecular signature of OC in dynamic mountainous river systems (Goñi et al., 2014).

The focus of this study is to assess the response of sediment and bulk OC to variability in seasonality and discharge behavior in a moderately steep river basin bridging the gap between headwater streams and lowland rivers. The sub-alpine Sihl River links small mountainous headwater streams with the higher-order river Limmat, providing a crucial window on downstream transport and the evolution of OC along the riverine continuum. We obtained a high-resolution time series over 40 months focusing on the content, composition ($\delta^{13}C$, $F^{14}C$), and flux of sediment and POC. Export fluxes are modeled using traditional and machine learning approaches, while a dual isotope model framework allows the estimation of potential organic matter source contributions. We discuss control mechanisms regulating organic matter mobilization and transport and examine our results in the context of previously published data on Sihl River headwater catchments in order to derive comparisons regarding the nature of exported POC (Smith et al., 2013; Turowski et al., 2016; Gies et al., 2022).

2 Methods

2.1 Characteristics of the Sihl River watershed

The Sihl River basin located in the Swiss Prealps is part of the Rhine River headwater system (4^{th} order tributary; **Fig. 1**). Its watershed covers an area of 346.0 km^2 ranging from an elevation of 1872 m (Druesberg) at its headwaters to 402 m at the catchment mouth, with an average slope of 19.5º (**Fig. 1a-b, Table 1**). The Sihl River basin experiences a humid continental climate with a mean annual air temperature of ~9.5ºC and annual precipitation varying from 1450 to 1830 mm, with snowfall generally occurring between November and April (MeteoSwiss, https://gate.meteoswiss.ch). The sub-alpine catchment is divided into an upper (145.7 km^2) and lower basin (190.1 km^2) near Einsiedeln by the reservoir Lake Sihl (10.2 km^2) constructed in 1937 (Addor et al., 2011). The damming of Lake Sihl results in the abrupt fragmentation of the flow path and the effective capture of 93% of sediment entrained from the upper watershed (Grill et al., 2019). The flow of the lower Sihl River is regulated by fourteen small-scale weir structures and four run-off-the-river hydroelectric systems. The Alp and Biber River tributaries are free-flowing rivers and major sources of water and sediment to the Sihl River. Similar to other small mountainous river systems (Wheatcroft et al., 2010), the steep morphology of the watershed and the absence of extensive floodplains limit the water and sediment storage capacity of the Sihl River. In response to severe storms, water discharge can rise from an average of 6.8 $m^3\ s^{-1}$ to over 200.0 $m^3\ s^{-1}$ and result in devastating flash floods (e.g., August 2005: 280.0 $m^3\ s^{-1}$; Bezzola and Hegg, 2007; Jaun and Ahrens, 2009).

The land cover of the Sihl River basin in 2017 consisted of 38.9 % meadows and pastures, 9.0 % urban settlements, 6.1 % unproductive areas (e.g., rock terrain), 1.3 % water bodies, and 1.1 % cropland (**Fig. 1c**; Federal Statistical Office, https://www.bfs.admin.ch), with the majority of the watershed covered by forests (43.4%; Waser et al., 2017). The main tree species in the upper basin are spruce (*Picea abies*) and fir (*Abies alba*) which are gradually replaced by deciduous trees such as beech (*Fagus sylvatica*), maple (*Acer spp.),* ash (*Fraxinus spp.),* and oak (*Quercus petraea*) in the lower basin (Schleppi et al., 2006). Forest soil carbon projections estimate stocks between 5 to 20 kgC m^{-2} (Nussbaum et al., 2014; van der Voort et al., 2019).

The lithology of the lower Sihl River basin is composed of weakly consolidated, clastic sediments of the Molasse basin (**Fig. 1d**; Swisstopo; https://www.swisstopo.admin.ch). Limestones and other biogenic sedimentary rocks are common in the allochthon nappes, Klippen, and Säntis zones. Campanian-Maastrichtian and Eocene flysch (Schlieren and Wägital flysch), largely composed of mudstone and calcareous sandstone, predominate in the Alp and upper Sihl River basins (Winkler et al., 1985). Dolomitic rocks of the northern limestone Alps and metamorphic rocks of the Arosa zone outcrop in the southern region of the upper Sihl River basin. Stream valleys and lowlands are filled with unconsolidated rock material such as alluvions, moraines, and gravel deposits that constitute important groundwater aquifers (Doppler et al., 2007).

The Erlenbach, Lümpenbach, and Vogelbach streams (**Fig. 1a**) are monitored as experimental catchments by the Swiss Federal Institute for Forest, Snow, and Landscape (WSL), and are well studied in terms of terrestrial OC sources, mobilization, and export of fine and coarse material (Schleppi et al., 1998; Hagedorn et al., 2001; Turowski et al., 2011, 2016; Rickenmann et al., 2012; Smith et al., 2013; Hilton et al., 2021; Gies et al., 2022). These streams are second-order tributaries to the Sihl River, with catchment sizes ranging from 0.7 to 1.6 km^2 and average discharges of 0.038 to 0.077 $m^3 s^{-1}$ (Smith et al., 2013; Gies et al., 2022). The Erlenbach basin is developed on an extensive bedrock landslide consisting primarily of Eocene Wägital flysch (Winkler et al., 1985; Schuerch et al., 2006; Golly et al., 2017), while bedrock lithologies in the Lümpenbach and Vogelbach are largely composed of calcareous sandstones (Milzow et al., 2006). The land cover of the drainage basins consists of alpine meadows, forests, and wetlands (Turowski et al., 2009; Gies et al., 2022).

2.2 Sample collection

From May 2014 to February 2015, surface water was sampled and processed by C. Freymond and H. Gies. Sample collection from August 2016 to March 2019 was designed to capture variations in OC export in response to both seasonal changes and shorter-term variations in discharge behavior. We collected surface water samples from the Sihl River (Allmend Park, 47.35º N, 8.52º E; **Fig. 1a**) in a biweekly rhythm using a river-rinsed bucket. In addition, river water was collected during seventeen storm events, emphasizing discharges >20 $m^3 s^{-1}$. Although the water level can rise ~1.7 m during exceptional flood events, the Sihl River is generally characterized by water depths <1 m suggesting little vertical variations in suspended sediment and POC concentrations in the water column. Surface waters were retrieved seasonally from Lake Sihl (Sihl River inflow and two locations in the center of the lake) and the Alp River (**Fig. 1a**).

Known volumes of surface water (0.95 to 64.61 L) were filtered through three pre-weighed and combusted (450ºC, 6 h) 90 or 142 mm glass microfiber filters (GF/F, Whatman) with a nominal pore size of 0.7 µm using a steel filtration unit. The filtration occurred either in the field or immediately upon returning to the laboratory at ETH. Filters were frozen after filtering and kept frozen until freeze-drying. Dried filters were re-weighed to obtain suspended sediment concentrations (SSC). We averaged water and sediment concentrations of the three collected filters to obtain a more robust representation of the suspended load. Filtered water was collected for DOC in 120 mL pre-combusted (450ºC, 6 h) amber bottles, acidified to pH 2 with 85 % H_3PO_4 (120 µL), and stored cooled (4º C) and in the dark. About 4 mL of filtrate was collected in glass vials for the analyses of water isotopic ($\delta^{18}O$, $\delta^{2}H$) compositions.

2.3 Geochemical analyses

Filter pieces (3 mm diameter) containing on average 350 µgC were placed in Ag boats (Säntis Analytical AG) and de-carbonated in a desiccator under HCl vapor (70º C, 72 h), followed by neutralization over NaOH pellets (70º C, 72 h; Freymond et al., 2018). Vapor-acid treated samples were wrapped in tin boats and analyzed for content and stable isotopic composition ($\delta^{13}C$) of OC using a coupled elemental analyzer-isotope ratio mass spectrometer (EA-IRMS, Elementar, Vario MICRO cube – Isoprime, VISION) system at the Laboratory of Ion Beam Physics (LIP) at ETH Zurich. Radiocarbon (^{14}C) was measured directly as CO_2 gas using a mini carbon dating system (MICADAS, Ionplus; Wacker et al., 2010; McIntyre et al., 2016). Samples were calibrated against Oxalic Acid II (NIST SRM 4990C) as well as an in-house soil and shale standards to correct for contamination during fumigation. All samples were corrected for constant contamination (~8 µgC) following Haghipour et al. (2019) and ^{14}C data are reported as fraction modern, $F^{14}C$ (Reimer et al., 2004).

A wet chemical oxidation approach was used to convert DOC into CO_2 (Lang et al., 2012, 2016). Due to low DOC concentrations in the Sihl River, 20 mL of sample material was concentrated in a pre-combusted 12 mL exetainer vial via repeated freeze-drying. The DOC (10-134 µgC) was then reconstituted in Milli-Q water, oxidized using an acidified sodium persulfate solution (100 mL H_2O + 4.0 g $Na_2S_2O_8$ + 200 µL of 85 % H_3PO_4), and purged at room temperature with high-purity helium gas (Grade 5.0, 99.9999% pure, for 10 min) removing ambient air and inorganic CO_2. The samples were then heated to 100º C for 1 h to convert the DOC to CO_2. Vials were loaded into the carbonate handling system of the MICADAS (LIP, ETH Zurich). Blank assessment was based on repeated measurements of sucrose (Sigma, $\delta^{13}C$: −12.4 ‰ VPDB, $F^{14}C$: 1.053±0.003) and phthalic acid (Sigma, $\delta^{13}C$: −33.6 ‰ VPDB, $F^{14}C$ <0.0025) standards, and process blanks. The evaluation of constant contamination amounted to ~2 µgC (Haghipour et al., 2019).

Analysis of water isotopic compositions ($\delta^{2}H$ and $\delta^{18}O$) was performed on a Picarro L2120-i cavity-ringdown spectrometer (Geological Institute, ETH). Standards comprised VSMOW2, GISP, and SLAP2 as well as three in-house reference waters. Each sample and reference material were injected seven times while discarding the first three injections to eliminate instrumental memory effects.

2.4 Bayesian isotope mixing model

We applied the MixSIAR unmixing approach to assess contributions of biogenic and petrogenic sources of the particulate OC load. MixSIAR is an open-source Bayesian tracer mixing model framework in the R computing environment that allows the estimation of fractional contributions of multiple sources to a mixture (Stock and Semmens, 2016; Stock et al., 2018). The model accounts for uncertainties in the source endmember compositions. Although mixing models were originally intended to constrain animal diets in ecology, they are often applied to apportion relative contributions of OC sources in rivers and lakes (Butman et al., 2015; Upadhayay et al., 2017; Repasch et al., 2021). We parameterized the mixing model using POC-$\delta^{13}C$, POC-$F^{14}C$, and five potential endmember compositions assessing the influence of seasonal and hydrodynamic variations on the source apportionment of organic matter in the Sihl River catchment. Organic carbon sources comprise bedrock, leaf litter, wood, top and deep soil material (Smith et al., 2013; van der Voort et al., 2016; Gies et al., 2022). The vegetation endmember ^{14}C composition was obtained by averaging reported atmospheric ^{14}C values from May 2014 to March 2019 (Hua et al., 2022). The soil endmember was divided based on a 10 cm threshold into a carbon-replete top and a carbon-poor deep mineral soil layer. We adjusted the ^{14}C signatures of soil samples collected in 1998 (van der Voort et al., 2016) to the sampling period using 2-point turnover calculations (van der Voort et al., 2019). Source endmember compositions are reported as OC-weighted mean and standard deviation (**Table B1**). However, as foliage, wood, top soils (<10 cm), and deep soils (>10 cm) are not statistically different in either $\delta^{13}C$ or $F^{14}C$ compositions, they are combined into a single biospheric endmember a priori. MixSIAR was run without any initial assumptions (uninformative prior), a burn-in of 200,000 iterations, a thinning factor of 100, and a chain length of 300,000 for three parallel Markov chain Monte Carlo chains. Model convergence was evaluated using Geweke (Geweke, 1991) and Gelman-Rubin metrics (Gelman and Rubin, 1992).

2.5 Estimating fluvial loads

2.5.1 Traditional sediment rating curves

River discharge is a key parameter determining the export of sediment and POC. Commonly, rating curves are used to calculate fluvial export where the sample collection is too infrequent to provide continuous concentration records. The relationship between concentration (C) data and discharge (Q) is fitted with a power law function (e.g., Walling, 1977; Cohn, 1995; Syvitski et al., 2000; Wheatcroft et al., 2010), $C=aQ^b\varepsilon$, where a and b are rating coefficients inferred from an ordinary least linear squares regression of logarithmically transformed data. However, log-transformed residuals introduce systematic bias that results in overestimation of small and underestimation of large values (Asselman, 2000; Cohn, 1995; Ferguson, 1986). We apply Duan's (1983) nonparametric retransformation bias correction factor (ε) appropriate for non-normal error distributions to minimize distortion:

$$\varepsilon = \frac{1}{N}\sum_{i=1}^{N} \exp\left(\ln(C) - \ln(aQ^b)\right) \quad (1)$$

Non-linear least squares regression does not require log-transformation as a power law function is directly fitted to the data. (Asselman, 2000). But this approach poses statistical problems as the assumption of homoscedasticity is often not met.

2.5.2 Machine learning approaches

Power rating curves are of limited value in predicting export fluxes as they rely largely on the relationship between discharge and the suspended load. In contrast, machine learning regressions enable the modeling of the dependent variable in response to several predictor variables. Although machine learning techniques gain increasing popularity in environmental and earth sciences (e.g., Karpatne et al., 2019; Reichstein et al., 2019), their application in fluvial hydrology remains limited (Olyaie et al., 2015; Choubin et al., 2018; Sharafati et al., 2020). Supervised machine learning refers to a set of data mining approaches that develop pattern recognition based on a sample dataset in order to predict unlabeled target values. Here, we applied four commonly used machine learning algorithms: a multiple linear regression (MLR), a support vector regression machine (SVR) (Drucker et al., 1997), a random forest regression (RFR) (Breiman, 2001), and a neural network regression (NNR) (McCulloch and Pitts, 1943). Detailed descriptions of the applied models can be found in **Appendix C**. We evaluated and compared different techniques with the goal of estimating annual sediment and POC fluxes for the Sihl River basin.

2.5.3 Predictor variables and parameterization

Power rating curves and machine learning regressions were developed based on data from physically collected sediment samples, as well as river discharge (Q), stage (H), precipitation (P), 1-day (P_{t-1}), and 2-day (P_{t-2}) antecedent precipitation (Choubin et al., 2018; Sharafati et al., 2020) spanning from 1974 to 2020 delineating sediment and POC export rates in the Sihl River. Daily discharge and water level values were obtained from the gauging station Sihlhölzli, Zurich, operated by the Swiss Federal Office for the Environment (FOEN, https://www.hydrodaten.admin.ch). Daily precipitation data was retrieved for 21 stations located within and around the Sihl River basin from the Federal Office of Meteorology and Climatology (MeteoSwiss, https://gate.meteoswiss.ch). We applied inverse distance weighted (IDW) interpolation to produce inclusive and comprehensive maps describing the distribution of daily rainfall in the Sihl River watershed. The IDW approach, without considering orography, assumes that the attributed value of an unknown point is the weighted average of known values within its neighborhood. Weights are inversely related to the distances between the predicted and sampled locations.

Machine learning models were developed using scikit-learn, an open software machine learning library for the Python programming language. Input variables were standardized using a robust scaler accounting for skewed data distributions and outliers. We tested several combinations of input predictors (**Table C1**) for machine learning approaches developing regression models. Hyperparameters for MLR, SVR, RFR, and NNR were determined using tuning techniques. Model tuning and stable model results were derived by 10-fold nested cross-validation (trials=20). The performance of each model to predict suspended

sediment and POC concentrations was evaluated based on three commonly used statistical metrics: the coefficient of determination (R^2), the root mean squared error (RMSE), and the mean absolute error (MAE). While the R^2 indicates the precision of the standard regression type, RMSE and MAE represent the model accuracy. All models were visually examined and compared using a combination of violin and strip plots, illustrating the probability and actual distributions of the observed and predicted data. The best-performing algorithms were chosen to interpolate annual sediment and OC export rates. Predicted sediment and POC concentration values of <0 were set to 0.

2.6 Statistical analyses

In order to statistically assess seasonal or rainfall-driven changes in exported sediment and OC concentrations and compositions, we introduce meteorological seasons and the discrimination between baseflow and stormflow conditions as categorical variables. A discharge threshold value of 12.7 $m^3 s^{-1}$ to separate stormflow from baseflow conditions was derived from the average daily flow duration curve of the Sihl River spanning 47 yr of continuous observation (**Fig. D1**). A flow duration curve represents the frequency of occurrence of various flow rates. Recorded discharges are ranked according to their magnitude and subdivided into the percentages of time during which specific flows are equaled or exceeded. Flow rates ranging from 0 to 10% exceedance are categorized as high flow events, while values above 90% indicate the contributions of groundwater to the streamflow.

Due to the assumption violations of normality, equal variances, and equal sample sizes, we performed non-parametric Mann-Whitney and Kruskal-Wallis rank-sum tests. After the identification of significant between-group differences, we applied Conover-Iman post hoc tests with a Bonferroni adjustment of *p*-values (**Table E1**). All statistical comparisons are reported at the 95 % confidence interval ($p<0.05$).

3 Results

3.1 Basin hydrology

Mean annual discharges observed during the study period (2016-2019) are comparable to the long-term mean value of Q_{mean} 6.8±0.1 $m^3 s^{-1}$ (M±SE). The lowest annual mean discharge is observed in 2018 (6.4±0.4 $m^3 s^{-1}$) reflecting prolonged periods of drought (Hari et al., 2020; Peters et al., 2020). The highest annual mean discharge amounts to 7.1±0.4 $m^3 s^{-1}$ in 2016. The sampled discharges range from 2.7 to 77 $m^3 s^{-1}$ and represent the full range of discharge conditions observed during the 40-month study period (**Fig. 2a; Fig. D1**). We observe no pronounced seasonal variability in the discharge of the Sihl River. Slight increases in water export coincide with snowmelt and periods of frequent storms in spring and summer (57 %). The majority of the annual discharge occurs during storm events (Q>12.7 $m^3 s^{-1}$; 82 %), while baseflow conditions account for only 18 %.

Riverine water isotopic compositions vary from -89.4 to -51.3 ‰ for δ^2H values and from -12.7 to -7.7 ‰ for $\delta^{18}O$ values (**Fig. 2c-d**, **3a**; **Table S1**). We note no difference between waters delivered during baseflow and stormflow conditions. However, water isotopic compositions are subject to seasonal shifts. While the majority of precipitation was primarily sourced from the North Atlantic, higher δ^2H and $\delta^{18}O$ values indicate enhanced moisture supply from terrestrial Mediterranean and locally recycled moisture sources during the summer months (LeGrande and Schmidt, 2006; Batibeniz et al., 2020).

3.2 Suspended sediment and organic carbon concentrations

Suspended sediment concentrations in the Sihl River range between 0.8 to 133.1 mg L^{-1}, with an average of 13.5±2.8 mg L^{-1} (n=77) during low flow conditions (**Fig. 3b**; **Table S1**). Suspended sediment concentrations reached an observed maximum of 398.3 mg L^{-1} (241.3±28.3 mg L^{-1}, n=17) during high discharge events. In comparison, SSC values of the Erlenbach varied from 19.8 to 15,310.7 mg L^{-1} during stormflow (Smith et al., 2013). We observe higher sediment input rates in fall (61.8±21.6 mg L^{-1}, n=29) and winter (64.8±25.8mg L^{-1}, n=25) compared to the spring (42.1±21.9 mg L^{-1}, n=17) and summer (44.1±11.6 mg L^{-1}, n=23) months. Suspended sediments collected from Lake Sihl and the Alp River show concentrations ranging from 1.2 to 82.2 mg L^{-1}.

Particulate OC concentrations range from 0.01 to 12.08 mgC L^{-1}, with an average concentration of 1.37±0.27 mgC L^{-1} (n=90, **Table S1**). Over an order of magnitude more organic matter is exported during storm-driven events (5.52±0.81 mgC L^{-1}, n=17) than during baseflow conditions (0.41±0.10 mgC L^{-1}, n=73). The observed range of suspended sediment OC contents vary from 0.37 to 11.64 wt% (2.48±0.18 wt%, n=92; **Fig. 2e**, **3c**). The mean POC content for low discharges amounts to 2.36±0.17 wt% (n=75), while POC content rapidly increases (3.02±0.63 wt%, n=17) during storm-driven events. In contrast to SSC, measured OC contents are lower during the fall (2.33±0.27 wt%, n=29) and winter (2.04±0.18 wt%, n=25) months, and increase to 2.84±0.75 wt% (n =15) in spring, and to 2.91±0.36 wt% in summer (n=23). The Sihl River transports higher POC contents compared to those reported for the Erlenbach by Smith et al. (2013; 1.45±0.06 wt%, n=122) and Gies et al. (2022; 1.79±0.34 wt%, n=24). In contrast, POC contents in the Lümpenbach and Vogelbach of ~5.35 wt% exceed those of the Sihl River (Gies et al., 2022). Observed POC concentrations and contents vary from 0.04 to 0.76 mg L^{-1} and from 0.89 to 2.13 wt% in Lake Sihl (n=15). Measured organic matter concentrations in the Alp River average 0.10±0.07 mg L^{-1} and OC contents to 2.58±0.24 wt% (n=3).

3.3 Isotopic composition of particulate and dissolved organic carbon

Sihl River POC-$\delta^{13}C$ signatures across the time-series range from -30.1 to -25.8 ‰, averaging -27.7±0.1 ‰ (n=92; **Fig. 2f**; **3d**; **Table S1**). No statistically significant differences between POC-$\delta^{13}C$ and discharge are observed, but we note pronounced seasonality in isotopic signatures (**Table D1**). Higher POC-$\delta^{13}C$ values are recorded during the summer (-27.1±0.1 ‰, n=23), whereas OC measured in spring exhibits on average the lowest $\delta^{13}C$ values (-28.1±0.2 ‰, n=17). In contrast, POC-$\delta^{13}C$ values in Lake Sihl (-29.7±0.5 ‰, n=15) and the Alp River (-28.0±0.3 ‰, n=2) are generally lower.

Bulk POC-$\delta^{13}C$ in the Sihl River overlaps with reported C_3 vegetation and soil biomass constituents (Kohn, 2010; Smith et al., 2013; Gies et al., 2022).

Sihl River POC-$F^{14}C$ values range from 0.56 to 1.00 (0.87±0.01, n=91; **Fig. 2g**; **Table S1**), and display a statistically significant positive correlation with discharge (r_S=0.43, p<0.001). Mean $F^{14}C$ values of 0.86±0.01 (n=75) are measured during low flow and increase to 0.91±0.01 (n=16; **Fig. 3e**) during high flow conditions. This indicates storm-driven mobilization and entrainment of undegraded, biospheric POC to the Sihl River, the latter having been observed in tectonically active regimes (Lyons et al., 2002; Carey et al., 2005; Hilton et al., 2008a, 2010; Gomez et al., 2010). In contrast, suspended sediment POC-$F^{14}C$ values in the mountainous Erlenbach average 0.65±0.08 (n=6) (Smith et al., 2013). Gies et al. (2022) report POC-$F^{14}C$ signatures for the Erlenbach, Lümpenbach, and Vogelbach of 0.64±0.22 (n=24), 0.80±0.17 (n=26), and 0.76±0.25 (n=27), respectively. The depletion in ^{14}C values in the Erlenbach likely reflects substantial contributions of petrogenic OC. Nevertheless, the overall OC-$F^{14}C$ values of Sihl River POC are in good agreement with forested, temperate catchments characterized by minor inputs of organic-rich sedimentary bedrock and the absence of intense agricultural land use (Raymond et al., 2004; Longworth et al., 2007; Goñi et al., 2013). The Alp River and Lake Sihl display POC-$F^{14}C$ values of 0.84±0.01 (n=3) and 0.79±0.02 (n=15).

DOC-$F^{14}C$ values vary from 0.52 to 1.16, with a mean of 0.95±0.01 (n=77; **Fig. 2h**, **3f; Table S1**). Moderately aged DOC is observed in the summer months (0.90±0.03, n=17), whereas DOC enriched in ^{14}C is discharged during fall (0.97±0.01, n=23). Similar to the $F^{14}C$ signature of POC, high precipitation events supply more modern DOC to the Sihl River (0.98±0.01, n=17). On average, Lake Sihl (0.97±0.01, n=15) and the Alp River (0.97±0.01, n=2) display slightly higher DOC-$F^{14}C$ signatures than the Sihl River.

3.4 Performance of predictive models

All four machine learning algorithms outperform traditional rating curve models (**Fig. 4**; **Fig. C1-2**) in predicting suspended sediment and POC concentrations. The statistical performance of the evaluated models according to different scenarios is listed in **Table C1**. Traditional rating curves overestimate low values of suspended sediment and POC leading to poor performance. Based on model performance criteria, SSC in the Sihl River depends primarily on discharge, water stage, and 1-day antecedent precipitation as predictor variables. Similar, scenarios that include discharge, water stage, precipitation, and 1-day antecedent precipitation appear to reliably reproduce measured POC concentrations. While discharge and water stage display the highest predictive power for instantaneous SSC, POC concentrations are more accurately described by water stage and 1-day antecedent precipitation. Random forest regression achieves the overall best fit with observed SSC (scenario 7; R^2=0.85, RMSE=39.0), followed by SVR (scenario 2; R^2=0.81, RMSE=43.8), MLR (scenario 8; R^2=0.80, RMSE=45.6), and NNR (scenario 2; R^2=0.75, RMSE=48.2). The highest coefficient of determination (R^2=0.73) and the lowest root mean squared error (RMSE=1.2) for predicting POC concentrations are obtained from SVR (scenario 4). The performance of NNR

(scenario 10; R^2=0.70, RMSE=1.4), RFR (scenario 8; R^2=0.68, RMSE=1.3), and MLR (scenario 8; R^2=0.59, RMSE=1.5) captured observed POC variations with less accuracy.

3.5 Annual fluxes and yields of suspended sediment and organic carbon

We calculate suspended sediment and POC export fluxes using continuous 47-year daily water discharge, stage, and precipitation records (see **Sect. 2.6**). Given our intermittent sampling design, we are not able to correct export fluxes for hysteresis effects or supply limitations (Wymore et al., 2019). We regard estimated sediment and POC budgets as conservative estimates, constraining a lower boundary.

Annual suspended sediment flux estimation for the Sihl River range from 17,790±1,042 (non-linear least squares power law) to 25,788±3,776 t yr^{-1} (bias-corrected power law) (**Table C2**). Fluxes provided by the best fitting model (RFR) average 25,167±1,056 t yr^{-1}. The majority of sediment export occurs during storm-driven events (72.9-93.0 %). We observe elevated export fluxes during summer (36.6-48.5 %) and spring (26.4-31.4 %) months corresponding to convective rainfall and snowmelt (Schmidt et al., 2019). The suspended sediment load in fall and winter varies between 12.0 and 18.4 % of the annual export. Similar to the export of suspended sediment, the lowest modeled annual POC flux (426±21 t yr^{-1}) is obtained from non-linear least squares power law functions, while bias-corrected rating curves provide the highest values (763±121 t yr^{-1}) (**Table C2**). The mean POC load inferred from the SVR model amounts to 574±25 t yr^{-1}. Particulate organic carbon is primarily mobilized and transported downstream during high discharge events (66.0-94.9 %). The highest POC loads are transported during summer (31.1-49.7 %) and spring (26.2-32.5 %), while lower fluxes are observed in fall and winter (11.5-18.3 %).

The reservoir Lake Sihl is considered a sediment trap, efficiently retaining particulate matter delivered from the upper Sihl River watershed. Therefore, mean annual yield calculations were restricted to the lower Sihl River basin, including the Alp and Biber catchments. We estimate annual yields between 93.6±5.5 and 135.7±19.9 t km^{-2} yr^{-1} (RFR: 132.4±5.6 t km^{-2} yr^{-1}) for suspended sediment and 2.2±0.1 and 4.0±0.6 t km^{-2} yr^{-1} (SVR: 3.0±0.1 t km^{-2} yr^{-1}) for POC.

4 Discussion

4.1 Seasonal variability in exported organic carbon

Rivers integrate a mixture of POC comprising contemporary organic matter derived from terrestrial and aquatic production, aged soil-derived organic matter, and OC devoid of ^{14}C released by weathered sedimentary bedrock (e.g., Hedges et al., 1986; Masiello and Druffel, 2001; Raymond et al., 2004; Blair and Aller, 2012). These sources have distinct carbon isotopic signatures and provide constraints on the contribution from different OC inputs. The Sihl River receives a uniform mixture of fresh, aged, and ancient OC pools with modest variations as seasons progress (**Fig. 5a**). MixSIAR modeling results suggest that suspended sediments in the Sihl River are largely derived from biospheric sources. The highest input of plant-derived

debris and soil material is supplied to the Sihl River watershed in spring (90±2 %, M±SD) followed by fall (88±2 %), winter (86±2 %), and summer (84±2 %). Similar source proportions have been observed in the headwaters of the Alp River (Gies et al., 2022).

Biospheric carbon sources consist of allochthonous (e.g., higher plant biomass, soils) and autochthonous (phytoplankton, benthic algae, aquatic macrophytes) inputs. However, we consider aquatic primary productivity as a negligible constituent of bulk particulate organic matter based on three considerations. First, the formation of large-scale phytoplankton blooms and microbial biofilms is likely restricted by the low abundance of nutrients (Känel et al., 2021; Romaní et al., 2004; Battin, 1999) and limited light conditions in forested river segments (Boston and Hill, 1991). Second, algal growth is further disturbed by high discharge events (when most of the POC is exported), resulting in river bed movement and the loss of algal mats (Schuwirth et al., 2008). Third, planktonic phytoplankton OC produced in Lake Sihl is efficiently retained by the hydroelectric dam (Grill et al., 2019). From the above reasoning, we believe that instream biomass does not contribute significant amounts of OC to the Sihl River and would not bias our interpretations.

Low POC-$\delta^{13}C$ values in winter and spring may indicate an enhanced input of leaf litter (-28.3±1.5 ‰; **Table B1**), while slightly more enriched values in the summer months may reflect contributions from freshwater C_3 plants ($\delta^{13}C$: ~-18 ‰; Chikaraishi, 2013), enhanced contributions of wood (-25.3±1.1 ‰) or soils (-26.9±1.1 ‰). However, the coarse-grained riverbed substrate prevents the colonization of macrophytes resulting in sparse aquatic vegetation in headwaters and allows only localized growth in the lower reaches of the Sihl River (Känel et al., 2021). We therefore attribute the ^{13}C enrichment in summer to increased entrainment of soil and wood debris. This interpretation is in agreement with soil erosion risk modeling based on the Revised Universal Soil Loss Equation (RUSLE) (Schmidt et al., 2016, 2019). Soil loss peaks between July and September in response to high rainfall erosivity on Swiss grasslands, while extensive vegetation cover is insufficient to counteract water-driven erosion (Schmidt et al., 2019, 2016).

Soils can often be partitioned into several endmembers reflecting different stages of soil development as aging, microbial decomposition, and respiration introduce alterations to the isotopic composition of organic matter (Fernandez et al., 2003; Werth and Kuzyakov, 2010; Wang et al., 2015). However, Swiss shallow soils frequently display relatively muted gradients in OC-^{14}C content with increasing soil depth and between climatic regions (van der Voort et al., 2016). This relatively homogenous isotopic composition has been ascribed to the presence of bomb-derived OC in soil layers up to 30 cm depth (van der Voort et al., 2016, 2019). Van der Voort et al. (2019) suggest that percolation of dissolved organic carbon (as constrained via water-extractable OC measurements) may serve as an agent to propagate modern carbon into deeper soil layers in nonwaterlogged (aerobic) soils, resulting in a less pronounced age gradient with depth. Additionally, roots and mycorrhizal communities may introduce bomb-derived OC to deeper soil layers. Physical and chemical soil erosion processes deliver primarily modern dissolved and particulate organic matter to the Sihl River, hindering source allocation between litter, top and deep soils.

The legacy of bomb-^{14}C is also evident in the DOC fractions retrieved from the Sihl River, which are consistently ^{14}C-enriched relative to corresponding POC samples (**Fig. 5b**). Commonly, DOC is leached from vegetation and soils by precipitation, and its residence time in fluvial systems is similar to that of water (Raymond and Bauer, 2001; Marwick et al., 2015). The overall modern OC-F^{14}C signature implies that DOC is primarily sourced from throughfall and the assimilation with non-fossil OC stored in litter and shallow soil layers (Inamdar et al., 2011, 2012). A recent study by von Freyberg et al. (2018) investigated the outflow of Swiss catchments and found that the residence time of contributing groundwater is less than 2-3 months. Similar to the Alp, Biber, Erlenbach and Vogelbach systems (von Freyberg et al., 2018), the Sihl River water isotopic compositions reflect seasonal cycles in precipitation and streamflow, implying that groundwater contributions are primarily sourced from recent rainfall events (**Fig. 2c-d**). The short residence time and the likely shallow flow paths result in limited fluid and solid interactions, impeding the dissolution and mobilization of moderately aged soil organic matter and favoring the export of percolating DOC derived from litter and organic-rich soil horizons.

Aged DOC is often associated with anthropogenic disturbances including deforestation, agriculture (Moore et al., 2013; Drake et al., 2019), atmospheric deposition (Stubbins et al., 2012; Spencer et al., 2014), and the release of petroleum and wastewater (Griffith et al., 2009; Regnier et al., 2013; Butman et al., 2015). Although we observe sporadic ^{14}C-depleted DOC signals collected during the summer months, which could be ascribed to the localized introduction of petrogenic OC emanating from fertilizers, mineral oil, or sewage, the majority of the DOC isotopic compositions suggest a generally low degree of anthropogenic disturbance.

4.2 Downstream evolution of particulate organic carbon

The isotopic composition of Lake Sihl (open symbols) in the upper watershed is distinctly different from the Sihl River (**Fig. 5a)**. While suspended sediment at the inlet of Lake Sihl (Lake Sihl 1) resembles material from the lower Sihl River, suspended sediments within the lake display more depleted ^{13}C and ^{14}C signatures. Lower POC-$\delta^{13}C$ values in lakes can be attributed to enhanced aquatic productivity. The ^{13}C isotopic composition of planktonic freshwater algae can range from -40 to -22 ‰ with the majority of reported $\delta^{13}C$ values being <-28 ‰ (Chikaraishi, 2013). Isotopic fractionation of phytoplankton biomass can be amplified in the presence of abundant dissolved inorganic carbon (DIC). Lake Sihl, a moderately alkaline waterbody, receives DIC from weathering carbonaceous bedrocks (Allochthon nappes, Northern limestone Alps, Säntis zone, **Fig. 1c**) via surface runoff and groundwater inflow. This “hard water effect” further manifests itself in lower POC-F^{14}C values as the input of bedrock-derived, ^{14}C-depleted DIC dilutes the carbon isotopic content of the water (Blattmann et al., 2019; Broecker and Walton, 1959; Keaveney and Reimer, 2012). Isotopic shifts in POC may also be caused by the selective uptake, decomposition, and preservation of organic matter (Lehmann et al., 2002, 2004). Kinetic isotope effects during enzymatic reactions lead to the enrichment or depletion of biomolecules relative to the bulk biomass (O’Leary, 1988). Carbohydrates and proteins often enriched in ^{13}C are bioactive compounds and preferentially decomposed by microbes (Harvey et al., 1995; van Dongen et al., 2002). In contrast, plant-derived lipids and lignin derived from plant

tissue exhibit in general lower $\delta^{13}C$ values and are more robust against degradation, leading to accumulation in the particulate fraction (Harvey et al., 1995; van Dongen et al., 2002; Lehmann and Kleber, 2015).

Surface water samples collected from Lake Sihl 1 in summer and Lake Sihl 2 in winter and spring are characterized by high SSC, low OC contents, and are enriched in ^{13}C, and depleted in ^{14}C (**Fig. 5a**). These signatures resemble those of the Sihl headwater streams (Smith et al., 2013; Gies et al., 2022) suggesting enhanced contributions of petrogenic OC (e.g., Wägital flysch). The suspended sediment was likely entrained by the Sihl and Minster Rivers in response to storm events, forming extensive sediment plumes in the epilimnion of Lake Sihl (**Fig. 1**). Fine-grained mineral soil- and bedrock-derived particles are advected to the center of the lake, whereas coarser, waterlogged biospheric debris mobilized by surface runoff is likely deposited near the river inlets (Douglas et al., 2022).

In comparison to the Sihl River, headwater-sourced POC is highly variable and encompasses a large range of carbon isotopic compositions (**Fig. 5a**, **6**). Headwaters, in particular the Erlenbach, receive substantial contributions of petrogenic OC (up to ~40 % of total OC) and fall between modern C_3 plants and bedrock endmembers (Smith et al., 2013; Gies et al., 2022). In a recent study, Hilton et al. (2021) used fluxes of dissolved Re, a redox-sensitive element, to constrain weathering intensities of petrogenic OC in the Erlenbach and Vogelbach basins. Findings suggest that ~40 % of OC contained in the Wägital flysch is lost to oxidative remineralization, implying that the majority of unweathered petrogenic POC is eroded and entrained into adjacent streams. Despite the high supply of sediment and petrogenic OC, the fingerprint of severely aged organic matter is gradually lost downstream. We attribute the gradual attenuation of headwater OC signals to (1) a declining input and increasingly distal source of bedrock-derived sediments, (2) an enhanced contribution of modern biospheric OC, (3) abiotic, and (4) biotic processes modifying organic matter during transit.

Highly erodible Eocene flysch sequences are superseded downstream by more competent Cretaceous flysch and molasse units, likely resulting in reduced erosion rates and a lower input of petrogenic OC. Simultaneously, the relative abundance of entrained litter and surface soils increases downstream, thereby diluting or replacing bedrock-derived particles (Feng et al., 2016; Hemingway et al., 2017). Numerous physicochemical mechanisms dynamically influence the addition, removal, and exchange of OC in dissolved and particulate pools. These processes include flocculation-deflocculation, particle sorption-desorption, aggregation-disaggregation, leaching, settling, and photo-oxidation (Bauer and Bianchi, 2012; Bianchi and Bauer, 2012). Flocculation and adsorption of largely modern DOC (**Fig. 5b**) onto particles may provide an additional source of biospheric organic matter further masking petrogenic OC inputs (von Wachenfeldt and Tranvik, 2008; Attermeyer et al., 2018).

Although rock-derived carbon is often regarded as inert, persisting in the environment for at least millennia, studies have shown that microbes in aquatic settings can assimilate and efficiently respire OC devoid of ^{14}C to CO_2 (Petsch et al., 2001; McCallister et al., 2004; Bouchez et al., 2010). However, flume experiments demonstrate that in-river transport, particle abrasion, and turbulent mixing exert minimal controls on the loss of organic matter, and that the preservation of OC is primarily regulated by transient storage in floodplains (Scheingross et al., 2019, 2021). Considering the absence of extensive floodplains

and the short-distance transport of water and sediment in the Sihl River watershed, we regard oxidative loss as a minor factor contributing to the removal of bedrock-sourced POC (Fox et al., 2020) and assume that overall OC fluxes experience little microbial decomposition during active fluvial transfer along the Alp-Sihl aquatic continuum.

The downstream exchange and dilution of petrogenic OC with relatively undegraded biospheric organic matter has previously been observed in large river systems such as the Amazon (Hedges et al., 1986, 2000; Mayorga et al., 2005), Ganges-Brahmaputra (Galy et al., 2008; Galy and Eglinton, 2011), Congo (Hemingway et al., 2017), and Orange Rivers (Herrmann et al., 2016). The alteration of riverine POC composition in these extensive river networks occurs over large spatial scales involving changes in topography, basin morphology, geology, vegetation, and climatic variables. In comparison, the Sihl River integrates and modifies exported POC over a ~40 km river interval without experiencing significant shifts in basin characteristics. These findings imply that low-order rivers may possess the potential to actively modulate exported OC impacting local and regional terrestrial carbon cycles.

4.3 Hydrologic controls on particulate organic carbon sources and pathways

MixSIAR model results suggest that storm-driven events mobilize and flush enhanced proportions of biospheric material into the Sihl River, with values rising from 85±1 % during baseflow to 90±2 % during high flow conditions. Concurrently, relative inputs of petrogenic OC decrease from 15±1 % to 10±1 %, respectively.

We observe pronounced patterns in the character of POC isotopic compositions as a function of discharge (**Fig. 6**). During low flow, POC-$\delta^{13}C$ and POC-$F^{14}C$ values display a large spread in values, corresponding to heterogeneous contributions from a variety of potential sources. In contrast, the isotopic signatures of storm-derived POC are less variable and appear to converge (as indicated by the arrows in **Fig. 6b-c**) towards a POC-$\delta^{13}C$ value of -27.5±0.1 ‰ and a POC-$F^{14}C$ value of 0.90±0.01. Similar behavior is noted in the Sihl headwaters (Gies et al., 2022). Although POC exhibits a larger variance in these headwaters, the composition of OC isotopes forms a relatively homogenous mixture during elevated precipitation events (Gies et al., 2022). This convergence might indicate a thorough mixing of several carbon pools mobilized during a storm event (Kao and Liu, 2000; Hilton et al., 2008a; Gies et al., 2022). However, high OC concentrations and predominately modern ^{14}C signatures of the Sihl River suspended load point towards a marked shift in sources and transport pathways from moderately aged to fresher organic carbon pools primarily consisting of surface soils and litter (**Fig. 3 c-d**).

The enhanced storm-facilitated export of modern biospheric material has been previously observed in subtropical (Hilton et al., 2008b, 2012; Wang et al., 2016; Qiao et al., 2020) and temperate regions (Medeiros et al., 2012; Hatten et al., 2012; Goñi et al., 2013), and has been attributed to increased surface runoff and landsliding. Heavy rainfall and the resulting overland flow mobilize and laterally transport loose plant-derived debris and sediment from surface soils to adjacent fluvial systems (Harmon et al., 1986; Medeiros et al., 2012; Hatten et al., 2012; Turowski et al., 2013). Storm-induced erosion processes such as shallow landslides efficiently detach litter and organic-rich surface soil layers and actively connect forested hillslopes to river channels

(Hovius et al., 2000; Hilton et al., 2011b, 2012). Storm events may also alter the relative contributions of distal and proximal OC sources. Rising water levels inundate adjacent riparian zones, potentially mobilizing significant amounts of standing riparian biomass, litter, and soil organic matter (Marwick et al., 2014; Sutfin et al., 2016). However, as the vegetation in the Sihl River watershed consists primarily of C_3 plants, the distinction between proximal and distal biospheric sources cannot be resolved by a simple dual OC isotopic approach.

The traditional rating curve exponent *b* is often interpreted as a proxy for the mobilization rate of particles in a fluvial system. However, the best-fit parameters for POC (1.9±0.1) and SSC (1.8±0.1) display similar values, suggesting no change in the ratio of exported OC to suspended sediment during elevated discharges.

In contrast, machine learning predictor variables differ in their ability to explain suspended sediment and POC concentrations, suggesting a divergence in sources and mobilization pathways. Discharge is a measure of the fluvial flow strength and the capacity to transport sediment downstream. Similarly, daily precipitation represents the intensity of rainfall and its potential to mobilize and laterally transfer particles via surface runoff. Water stage may act as a proxy for inundation as flooding links the river channel with banks and the adjacent floodplain supporting the mobilization of loosely held sediment and plant-derived debris.

The applied machine learning algorithms rely primarily on discharge and water stage to predict SSC in the Sihl River (**Table C1**). This dependency may indicate that the majority of carbon-poor sediment is sourced from channel beds and banks. The variables water stage and 1-day antecedent precipitation achieve high predictive performance for POC concentrations and may suggest that flooding and precipitation-induced erosion are major mechanisms facilitating the export of coarse discrete organic carbon via detaching litter and surface soil. This interpretation agrees with previous assessments by Smith et al. (2013) for the Erlenbach stream, highlighting the importance of overland flow for POC export.

4.4 Export fluxes and implications

Sediment fluxes in the Sihl River basin are less than half of the particle export documented in other Swiss Rivers (Spreafico et al., 2005). The low yield can be attributed to (1) the damming of the upper basin (Lake Sihl), retaining annually up to 1470 t yr^{-1} of the suspended sediment load (Spreafico, 2007), (2) river engineering, (3) topography, and (4) catchment geology.

Although the course of the Sihl River is strongly engineered, with four run-off-the-river hydroelectric systems and fourteen weir structures, these artificial barriers pose only minor obstructions to water and sediment export. Run-off-the-river systems use the natural flow rate of the river by redirecting a portion of the river water through a penstock to a turbine (Csiki and Rhoads, 2010). The water is then returned to the main channel further downstream. Weirs or overflow dams are barriers that do not exceed the elevation of the channel banks allowing constant flow over the weir crest during baseflow conditions. Weirs along the Sihl River consist largely of broad-crested weirs, boulder weirs, and water stairs. In comparison to large

dams that inundate the river channel and floodplain, run-off-the-river and weir structures create low-head impoundments with little or no storage capacity and present no effective barriers against flooding. Instead, partly fortified river banks and the narrow floodplain of the Sihl River basin (<10 %; Grill et al., 2019) likely support the routing of water and sediment downstream during storm-driven events.

Differences in bedrock lithology influence the export of sediment and associated petrogenic OC. The lithology in the lower watershed consists mainly of molasse characterized by low slope angles and a reduced erosion potential (Schuerch et al., 2006; Korup and Schlunegger, 2009). Only the Alp River drains highly erosive flysch formations in the lower Sihl River basin (Winkler et al., 1985). However, flysch units differ markedly in their erosivity. While the Erlenbach is underlain by easily erodible, fine-grained Eocene pelitic turbidites and mudstone sequences, bedrock in the Lümpenbach and Vogelbach watersheds mainly consist of more competent Cretaceous calcareous sandstones (**Fig. 1d**) (Keller and Weibel, 1991; Milzow et al., 2006; Schuerch et al., 2006). These differences in lithological units are manifested in their respective sediment yields. The Erlenbach, despite comprising only 0.4 % of the lower Sihl River basin, supplies about 4.7 to 6.7 % of the overall particulate load, with mean annual sediment yields ranging from 1225 to 1648 t km^{-2} y^{-1} (Keller and Weibel, 1991; Smith et al., 2013). In comparison, the watershed of the Vogelbach is twice as large as the Erlenbach but has similar SSC export flux rates (4.4-6.4 %), resulting in lower annual sediment yields of 725 t km^{-2} yr^{-1} (Keller and Weibel, 1991).

By multiplying OC fluxes with the mean values of the MixSIAR posterior distributions for baseflow and stormflow conditions, while neglecting contributions from in-situ aquatic productivity, we can estimate export rates for the contributions of biospheric and petrogenic OC. Biospheric (2.0-3.6 tC km^{-2} yr^{-1}) and petrogenic (0.3-0.4 tC km^{-2} yr^{-1}) POC yields in the Sihl River are similar to contributions from the Erlenbach reported by Gies et al. (2022; POC_{bio}: 1.2±0.4 tC km^{-2} yr^{-1}) but distinctly lower than estimations by Smith et al. (2013) (POC_{bio}: 14.0±4.4 tC km^{-2} yr^{-1}, POC_{petro}: 10.1±1.6 tC km^{-2} yr^{-1}). Smith et al. (2013) focused their sample collection on storm-driven events yielding particularly high export fluxes, and this may account for the discrepancy in fluxes. However, the increase in relative biospheric contributions concomitant with the reduction in petrogenic OC proportions, and the decline in absolute export yields from headwaters to the downstream Sihl sampling site, underline the impact of diverse processes acting upon and contributing to OC along the fluvial continuum. These processes reflect the impact of subtle changes in basin lithology (erosivity, OC content), geomorphology (slope, floodplain extent), and anthropogenic activities (e.g., damming, channelization, land-use) on the age and the composition of exported POC.

5 Conclusions

This study focuses on temporal variations in organic carbon export from a Swiss subalpine river and its tributary streams, and provides insights into the mechanisms of sediment and associated OC mobilization and transport within a moderately steep river basin. Our results indicate that POC in the Sihl River consists primarily of modern to moderately aged biospheric OC derived from terrestrial vegetation and soils. While petrogenic carbon is prevalent in Sihl headwater catchments, the signal is

gradually lost downstream. We attribute this decline of rock-derived OC to decreasing contributions of source material that are restricted to upstream segments of the watershed, and to dilution and replacement by soil and plant biomass, and instream OC transformation processes. Despite the moderate stream gradient of the Sihl River, particle export is driven by episodic, short-lived storm events. We observe large variations in the isotopic composition of organic matter during baseflow conditions, whereas POC-$\delta^{13}C$ and POC-$F^{14}C$ values converge to a more uniform mixture during storm-driven events. Results of traditional and machine learning modeling approach further reveal diverging transport pathways for suspended sediment and OC with increasing discharge. Given the high POC content, the modern POC-$F^{14}C$ signature, and the differences in particle mobilization, we suggest that severe precipitation events facilitate the preferential entrainment of litter and surficial soil layers via surface runoff or the inundation of riparian vegetation and soils. Climate model simulations predict an increase in intensity, frequency, and duration of extreme precipitation events both regionally and globally with continued climate warming (Myhre et al., 2019; Kahraman et al., 2021) resulting in enhanced flood risks, water-induced erosion, and landsliding. The increased export of freshwater, nutrients, and sediment will likely severely affect downstream ecosystems, carbon cycling, requiring direct human intervention (Turowski et al., 2009; Talbot et al., 2018), and warranting the continuous monitoring of river systems.

Appendix A: Dissolved organic carbon concentrations

DOC concentration measurements were conducted using a Shimadzu system (TOC-L Series) at the Department of Environmental System Science at ETH Zurich and are reported in **Table S1**. However, measurements from August 2016 to March 2018 are not reported due to uncertainties in the quality of the measurements. We choose not to discuss them in the manuscript.

Appendix B: Endmember compositions for the Bayesian unmixing model (MixSIAR)

Appendix C: Machine learning approaches

Multiple linear regression (MLR) assumes a linear relationship between a single dependent continuous variable and several independent variables. To reduce overfitting of the MLR, we apply Elastic Net regularization which penalizes the model for both ℓ_1 and ℓ_2-norms (Zou and Hastie, 2005).

Support vector regressions (SVR) are a popular machine learning approach performing linear or nonlinear classification, regression, and outlier detection. The support vector machine classification algorithm identifies an optimal hyperplane in n-dimensional space to separate and categorize data points. In contrast, the SVR uses this principle to fit as many instances onto a hyperplane while limiting margin violations. This supervised learning algorithm supports different kernels (linear, gaussian

radial basis, polynomial) handling nonlinearity. Radial basis function kernels are commonly applied to fit non-linear regression lines and often outperform linear and polynomial kernels.

A standard decision tree is a non-parametric supervised learning method that predicts the value of a target variable by inferring simple decision rules based on data features. Decision trees are prone to overfitting the training set and thus are often replaced by an ensemble of decision trees called a random forest. Random forests are generally built on bagging and random feature selection creating an uncorrelated forest of decision trees and thus generalizing well to unseen data (Breiman, 2001).

Neural Networks are a system of algorithms inspired by the human brain that attempts to recognize underlying patterns in a data set. The simplest neural network consists of an input and output layer that is interconnected through one hidden layer. Each neuron in these layers has an associated weight and threshold. The weighted sum of all neurons in a layer is passed through an activation function and augmented by a bias term. In a feed-forward neural network, backpropagation adjusts the weights by minimizing the loss function and reducing the error between modeled and output values (Rumelhart et al., 1986). The utilized architecture consists of two hidden layers containing each ten neurons. To prevent overfitting, we apply dropout. This regularization technique temporarily removes units during the training period (Srivastava et al., 2014). Dropped units are chosen randomly.

Appendix D: Flow duration curve

Appendix E: Results of non-parametric analyses of variance

Data availability

All data generated are openly available in the EarthChem Library via https://doi.org/10.26022/IEDA/112503.

Supplement

Supporting information is available for this paper

Author contributions

MSS, ML, and TIE led the design of the study. HG and CF led data collection and analyses from 2014 to 2015. MSS conducted field and lab work from 2016 to 2019, data analysis and interpretation. NH contributed to laboratory analyses. MSS prepared the manuscript with contributions from all co-authors.

Competing interests

The authors declare that they have no conflict of interest.

Acknowledgments

We thank Francien Peterse for her motivation to initiate time-series sampling of the Sihl River. We thank Lena Märki for sample collection and Daniel Montluçon for laboratory assistance.

Financial support

M.S.S. was supported by the Swiss National Science Foundation through the grants SNF200020_163162/1, "CAPS-LOCK II" and SNF200020_184865/1, "CAPS-LOCK III".

References

Addor, N., Jaun, S., Fundel, F., and Zappa, M.: An operational hydrological ensemble prediction system for the city of Zurich (Switzerland): skill, case studies and scenarios, Hydrol Earth Syst Sci, 15, 2327–2347, https://doi.org/10.5194/hess-15-2327-2011, 2011.

Asselman, N. E. M.: Fitting and interpretation of sediment rating curves, J Hydrol (Amst), 234, 228–248, https://doi.org/10.1016/S0022-1694(00)00253-5, 2000.

Attermeyer, K., Catalán, N., Einarsdottir, K., Freixa, A., Groeneveld, M., Hawkes, J. A., Bergquist, J., and Tranvik, L. J.: Organic Carbon Processing During Transport Through Boreal Inland Waters: Particles as Important Sites, J Geophys Res Biogeosci, 123, 2412–2428, https://doi.org/10.1029/2018JG004500, 2018.

Aufdenkampe, A. K., Mayorga, E., Raymond, P. A., Melack, J. M., Doney, S. C., Alin, S. R., Aalto, R. E., and Yoo, K.: Riverine coupling of biogeochemical cycles between land, oceans, and atmosphere, Front Ecol Environ, 9, 53–60, https://doi.org/10.1890/100014, 2011.

Batibeniz, F., Ashfaq, M., Önol, B., Turuncoglu, U. U., Mehmood, S., and Evans, K. J.: Identification of major moisture sources across the Mediterranean Basin, Clim Dyn, 54, 4109–4127, https://doi.org/10.1007/s00382-020-05224-3, 2020.

Battin, T. J.: Hydrologic flow paths control dissolved organic carbon fluxes and metabolism in an alpine stream hyporheic zone, Water Resour Res, 35, 3159–3169, https://doi.org/10.1029/1999WR900144, 1999.

Battin, T. J., Luyssaert, S., Kaplan, L. A., Aufdenkampe, A. K., Richter, A., and Tranvik, L. J.: The boundless carbon cycle, Nat Geosci, 2, 598–600, https://doi.org/10.1038/ngeo618, 2009.

Bauer, J. E. and Bianchi, T. S.: Dissolved Organic Carbon Cycling and Transformation, in: Treatise on Estuarine and Coastal Science, vol. 5, Elsevier Inc., 7–67, https://doi.org/10.1016/B978-0-12-374711-2.00502-7, 2012.

Bezzola, G. R. and Hegg, C.: Ereignisanalyse Hochwasser 2005, Teil 1 - Prozessse, Schäden und erste Einordnung, Umwelt Wissen, 0707, 215, https://doi.org/Umwelt-Wissen Nr. 0707, 2007.

Bianchi, T. S. and Bauer, J. E.: Particulate Organic Carbon Cycling and Transformation, in: Treatise on Estuarine and Coastal Science, vol. 5, Elsevier Inc., 69–117, https://doi.org/10.1016/B978-0-12-374711-2.00503-9, 2012.

Blair, N. E. and Aller, R. C.: The Fate of Terrestrial Organic Carbon in the Marine Environment, Ann Rev Mar Sci, 4, 401–423, https://doi.org/10.1146/annurev-marine-120709-142717, 2012.

Blair, N. E., Leithold, E. L., Ford, S. T., Peeler, K. A., Holmes, J. C., and Perkey, D. W.: The persistence of memory: The fate of ancient sedimentary organic carbon in a modern sedimentary system, Geochim Cosmochim Acta, 67, 63–73, https://doi.org/10.1016/S0016-7037(02)01043-8, 2003.

Blattmann, T. M., Wang, S. L., Lupker, M., Märki, L., Haghipour, N., Wacker, L., Chung, L. H., Bernasconi, S. M., Plötze, M., and Eglinton, T. I.: Sulphuric acid-mediated weathering on Taiwan buffers geological atmospheric carbon sinks, Sci Rep, 9, https://doi.org/10.1038/s41598-019-39272-5, 2019.

Boston, H. L. and Hill, W. R.: Photosynthesis-light relations of stream periphyton communities, Limnol. Oceanogr, 644–656 pp., 1991.

Bouchez, J., Beyssac, O., Galy, V. v., Gaillardet, J. J., France-Lanord, C., Maurice, L., Moreira, and Moreira-Turcq, P.: Oxidation of petrogenic organic carbon in the Amazon floodplain as a source of atmospheric CO_2, Geology, 38, 255–258, https://doi.org/10.1130/G30608.1, 2010.

Breiman, L.: Random Forests, Mach Learn, 45, 5–32, https://doi.org/10.1007/978-3-030-62008-0_35, 2001.

Broecker, W. S. and Walton, A.: The Geochemistry of ^{14}C in Freshwater Systems, Geochim Cosmochim Acta, 16, 15–38, 1959.

Butman, D. E., Wilson, H. F., Barnes, R. T., Xenopoulos, M. A., and Raymond, P. A.: Increased mobilization of aged carbon to rivers by human disturbance, Nat Geosci, 8, 112–116, https://doi.org/10.1038/ngeo2322, 2015.

Carey, A. E., Gardner, C. B., Goldsmith, S. T., Lyons, W. B., and Hicks, D. M.: Organic carbon yields from small, mountainous rivers, New Zealand, Geophys Res Lett, 32, 1–5, https://doi.org/10.1029/2005GL023159, 2005.

Chikaraishi, Y.: $^{13}C/^{12}C$ Signatures in Plants and Algae, in: Treatise on Geochemistry: Second Edition, vol. 12, Elsevier Ltd., 95–123, https://doi.org/10.1016/B978-0-08-095975-7.01008-1, 2013.

Choubin, B., Darabi, H., Rahmati, O., Sajedi-Hosseini, F., and Kløve, B.: River suspended sediment modelling using the CART model: A comparative study of machine learning techniques, Science of the Total Environment, 615, 272–281, https://doi.org/10.1016/j.scitotenv.2017.09.293, 2018.

Cohn, T. A.: Recent advances in statistical methods for the estimation of sediment and nutrient transport in rivers, Reviews of Geophysics, 33, 1117–1123, https://doi.org/10.1029/95RG00292, 1995.

Cole, J. J., Prairie, Y. T., Caraco, N. F., McDowell, W. H., Tranvik, L. J., Striegl, R. G., Duarte, C. M., Kortelainen, P., Downing, J. A., Middelburg, J. J., and Melack, J.: Plumbing the global carbon cycle: Integrating inland waters into the terrestrial carbon budget, Ecosystems, 10, 171–184, https://doi.org/10.1007/s10021-006-9013-8, 2007.

Coynel, A., Etcheber, H., Abril, G., Maneux, E., Dumas, J., and Hurtrez, J. E.: Contribution of small mountainous rivers to particulate organic carbon input in the Bay of Biscay, Biogeochemistry, 74, 151–171, https://doi.org/10.1007/s10533-004-3362-1, 2005.

Csiki, S. and Rhoads, B. L.: Hydraulic and geomorphological effects of run-of-river dams, Prog Phys Geogr, 34, 755–780, https://doi.org/10.1177/0309133310369435, 2010.

van Dongen, B. E., Schouten, S., and Sinninghe Damsté, J. S.: Carbon isotope variability in monosaccharides and lipids of aquatic algae and terrestrial plants, Mar Ecol Prog Ser, 232, 83–92, https://doi.org/10.3354/meps232083, 2002.

Doppler, T., Franssen, H. J. H., Kaiser, H. P., Kuhlman, U., and Stauffer, F.: Field evidence of a dynamic leakage coefficient for modelling river-aquifer interactions, J Hydrol (Amst), 347, 177–187, https://doi.org/10.1016/j.jhydrol.2007.09.017, 2007.

Douglas, P. M. J., Stratigopoulos, E., Park, S., and Keenan, B.: Spatial differentiation of sediment organic matter isotopic composition and inferred sources in a temperate forest lake catchment, Chem Geol, 603, https://doi.org/10.1016/j.chemgeo.2022.120887, 2022.

Drake, T. W., van Oost, K., Barthel, M., Bauters, M., Hoyt, A. M., Podgorski, D. C., Six, J., Boeckx, P., Trumbore, S. E., Cizungu Ntaboba, L., and Spencer, R. G. M.: Mobilization of aged and biolabile soil carbon by tropical deforestation, Nat Geosci, 12, 541–546, https://doi.org/10.1038/s41561-019-0384-9, 2019.

Drucker, H., Surges, C. J. C., Kaufman, L., Smola, A., and Vapnik, V.: Support vector regression machines, in: Advances in Neural Information Processing Systems, 155–161, 1997.

Duan, N.: Smearing estimate: A nonparametric retransformation method, J Am Stat Assoc, 78, 605–610, https://doi.org/10.1080/01621459.1983.10478017, 1983.

Feng, X., Feakins, S. J., Liu, Z., Ponton, C., Wang, R. Z., Karkabi, E., Galy, V., Berelson, W. M., Nottingham, A. T., Meir, P., and West, A. J.: Source to sink: Evolution of lignin composition in the Madre de Dios River system with connection to the Amazon basin and offshore, Journal of Geophysical Research G: Biogeosciences, 121, 1316–1338, https://doi.org/10.1002/2016JG003323, 2016.

Ferguson, R. I.: River Loads Underestimated by Rating Curves, Water Resour Res, 22, 74–76, https://doi.org/10.1029/WR022i001p00074, 1986.

Fernandez, I., Mahieu, N., and Cadisch, G.: Carbon isotopic fractionation during decomposition of plant materials of different quality, Global Biogeochem Cycles, 17, https://doi.org/10.1029/2001gb001834, 2003.

Fox, P. M., Bill, M., Heckman, K., Conrad, M., Anderson, C., Keiluweit, M., and Nico, P. S.: Shale as a Source of Organic Carbon in Floodplain Sediments of a Mountainous Watershed, J Geophys Res Biogeosci, 125, https://doi.org/10.1029/2019JG005419, 2020.

von Freyberg, J., Allen, S. T., Seeger, S., Weiler, M., and Kirchner, J. W.: Sensitivity of young water fractions to hydro-climatic forcing and landscape properties across 22 Swiss catchments, Hydrol Earth Syst Sci, 22, 3841–3861, https://doi.org/10.5194/hess-22-3841-2018, 2018.

Freymond, C. v., Lupker, M., Peterse, F., Haghipour, N., Wacker, L., Filip, F., Giosan, L., and Eglinton, T. I.: Constraining Instantaneous Fluxes and Integrated Compositions of Fluvially Discharged Organic Matter, Geochemistry, Geophysics, Geosystems, 19, 2453–2462, https://doi.org/10.1029/2018GC007539, 2018.

Galy, V. and Eglinton, T.: Protracted storage of biospheric carbon in the Ganges-Brahmaputra basin, Nat Geosci, 4, 843–847, https://doi.org/10.1038/ngeo1293, 2011.

Galy, V., France-Lanord, C., and Lartiges, B.: Loading and fate of particulate organic carbon from the Himalaya to the Ganga-Brahmaputra delta, Geochim Cosmochim Acta, 72, 1767–1787, https://doi.org/10.1016/j.gca.2008.01.027, 2008.

Gelman, A. and Rubin, D. B.: Inference form Iterative Simulation Using Multiple Sequences, Statistical Science, 7, 457–472, 1992.

Geweke, J.: Evaluating the accuracy of sampling-based approaches to the calculation of posterior moments., No. 148. Federal Reserve Bank of Minneapolis., 30 pp., 1991.

Gies, H., Lupker, M., Wick, S., Haghipour, N., Buggle, B., and Eglinton, T.: Discharge-Modulated Soil Organic Carbon Export From Temperate Mountainous Headwater Streams, J Geophys Res Biogeosci, 127, https://doi.org/10.1029/2021JG006624, 2022.

Golly, A., Turowski, J. M., Badoux, A., and Hovius, N.: Controls and feedbacks in the coupling of mountain channels and hillslopes, Geology, 45, 307–310, https://doi.org/10.1130/G38831.1, 2017.

Gomez, B., Baisden, W. T., and Rogers, K. M.: Variable composition of particle-bound organic carbon in steepland river systems, J Geophys Res Earth Surf, 115, 1–9, https://doi.org/10.1029/2010JF001713, 2010.

Goñi, M. A., Hatten, J. A., Wheatcroft, R. A., and Borgeld, J. C.: Particulate organic matter export by two contrasting small mountainous rivers from the Pacific Northwest, U.S.A., J Geophys Res Biogeosci, 118, 112–134, https://doi.org/10.1002/jgrg.20024, 2013.

Goñi, M. A., Moore, E., Kurtz, A., Portier, E., Alleau, Y., and Merrell, D.: Organic matter compositions and loadings in soils and sediments along the Fly River, Papua New Guinea, Geochim Cosmochim Acta, 140, 275–296, https://doi.org/10.1016/j.gca.2014.05.034, 2014.

Griffith, D. R., Barnes, R. T., and Raymond, P. A.: Inputs of fossil carbon from wastewater treatment plants to U.S. Rivers and oceans, Environ Sci Technol, 43, 5647–5651, https://doi.org/10.1021/es9004043, 2009.

Grill, G., Lehner, B., Thieme, M., Geenen, B., Tickner, D., Antonelli, F., Babu, S., Borrelli, P., Cheng, L., Crochetiere, H., Ehalt Macedo, H., Filgueiras, R., Goichot, M., Higgins, J., Hogan, Z., Lip, B., McClain, M. E., Meng, J., Mulligan, M., Nilsson, C., Olden, J. D., Opperman, J. J., Petry, P., Reidy Liermann, C., Sáenz, L., Salinas-Rodríguez, S., Schelle, P., Schmitt, R. J. P., Snider, J., Tan, F., Tockner, K., Valdujo, P. H., van Soesbergen, A., and Zarfl, C.: Mapping the world's free-flowing rivers, Nature, 569, 215–221, https://doi.org/10.1038/s41586-019-1111-9, 2019.

Hagedorn, F., Bucher, J. B., and Schleppi, P.: Contrasting dynamics of dissolved inorganic and organic nitrogen in soil and surface waters of forested catchments with Gleysols, Geoderma, 100, 173–192, https://doi.org/10.1016/S0016-7061(00)00085-9, 2001.

Haghipour, N., Ausin, B., Usman, M. O., Ishikawa, N., Wacker, L., Welte, C., Ueda, K., and Eglinton, T. I.: Compound-Specific Radiocarbon Analysis by Elemental Analyzer-Accelerator Mass Spectrometry: Precision and Limitations, Anal Chem, 91, 2042–2049, https://doi.org/10.1021/acs.analchem.8b04491, 2019.

Hari, V., Rakovec, O., Markonis, Y., Hanel, M., and Kumar, R.: Increased future occurrences of the exceptional 2018–2019 Central European drought under global warming, Sci Rep, 10, 1–10, https://doi.org/10.1038/s41598-020-68872-9, 2020.

Harmon, M. E., Franklin, J. F., Swanson, F. J., Sollins, P., Gregory, S. v., Lattin, J. D., Anderson, N. H., Cline, S. P., Aumen, N. G., Sedell, J. R., Lienkaemper, G. W., Cromack, K., and Cummins, K. W.: Ecology of Coarse Woody Debris in Temperate Ecosystems, Adv Ecol Res, 15, 133–302, https://doi.org/10.1016/S0065-2504(03)34002-4, 1986.

Harvey, H. R., Tuttle, J. H., and Bell, J. T.: Kinetics of phytoplankton decay during simulated sedimentation: Changes in biochemical composition and microbial activity under oxic and anoxic conditions, Geochim Cosmochim Acta, 59, 3367–3377, https://doi.org/10.1016/0016-7037(95)00217-N, 1995.

Hatten, J. A., Goñi, M. A., and Wheatcroft, R. A.: Chemical characteristics of particulate organic matter from a small, mountainous river system in the Oregon Coast Range, USA, Biogeochemistry, 107, 43–66, https://doi.org/10.1007/s10533-010-9529-z, 2012.

Hedges, J. I., Clark, W. A., Quay, P. D., Richey, J. E., Devol, A. H., and Santos, U. D. M.: Compositions and fluxes of particulate organic material in the Amazon River, Limnol Oceanogr, 31, 717–738, https://doi.org/10.4319/lo.1986.31.4.0717, 1986.

Hedges, J. I., Mayorga, E., Tsamakis, E., McClain, M. E., Aufdenkampe, A., Quay, P., Richey, J. E., Benner, R., Opsahl, S., Black, B., Pimentel, T., Quintanilla, J., and Maurice, L.: Organic matter in Bolivian tributaries of the Amazon River: A comparison to the lower mainstream, Limnol Oceanogr, 45, 1449–1466, https://doi.org/10.4319/lo.2000.45.7.1449, 2000.

Hemingway, J. D., Schefuß, E., Spencer, R. G. M., Dinga, B. J., Eglinton, T. I., McIntyre, C., and Galy, V. v.: Hydrologic controls on seasonal and inter-annual variability of Congo River particulate organic matter source and reservoir age, Chem Geol, 466, 454–465, https://doi.org/10.1016/j.chemgeo.2017.06.034, 2017.

Herrmann, N., Boom, A., Carr, A. S., Chase, B. M., Granger, R., Hahn, A., Zabel, M., and Schefuß, E.: Sources, transport and deposition of terrestrial organic material: A case study from southwestern Africa, Quat Sci Rev, 149, 215–229, https://doi.org/10.1016/j.quascirev.2016.07.028, 2016.

Hilton, R. G., Galy, A., and Hovius, N.: Riverine particulate organic carbon from an active mountain belt: Importance of landslides, Global Biogeochem Cycles, 22, 1–12, https://doi.org/10.1029/2006GB002905, 2008a.

Hilton, R. G., Galy, A., Hovius, N., Chen, M.-C., Horng, M.-J., and Chen, H.: Tropical-cyclone-driven erosion of the terrestrial biosphere from mountains, Nat Geosci, 1, 759–762, https://doi.org/10.1038/ngeo333, 2008b.

Hilton, R. G., Galy, A., Hovius, N., Horng, M. J., and Chen, H.: The isotopic composition of particulate organic carbon in mountain rivers of Taiwan, Geochim Cosmochim Acta, 74, 3164–3181, https://doi.org/10.1016/j.gca.2010.03.004, 2010.

Hilton, R. G., Galy, A., Hovius, N., Horng, M. J., and Chen, H.: Efficient transport of fossil organic carbon to the ocean by steep mountain rivers: An orogenic carbon sequestration mechanism, Geology, 39, 71–74, https://doi.org/10.1130/G31352.1, 2011a.

Hilton, R. G., Meunier, P., Hovius, N., Bellingham, P. J., and Galy, A.: Landslide impact on organic carbon cycling in a temperate montane forest, Earth Surf Process Landf, 36, 1670–1679, https://doi.org/10.1002/esp.2191, 2011b.

Hilton, R. G., Galy, A., Hovius, N., Kao, S. J., Horng, M. J., and Chen, H.: Climatic and geomorphic controls on the erosion of terrestrial biomass from subtropical mountain forest, Global Biogeochem Cycles, 26, 1–12, https://doi.org/10.1029/2012GB004314, 2012.

Hilton, R. G., Turowski, J. M., Winnick, M., Dellinger, M., Schleppi, P., Williams, K. H., Lawrence, C. R., Maher, K., West, M., and Hayton, A.: Concentration-Discharge Relationships of Dissolved Rhenium in Alpine Catchments Reveal Its Use as a Tracer of Oxidative Weathering, Water Resour Res, 57, https://doi.org/10.1029/2021WR029844, 2021.

Hovius, N., Stark, C. P., Hao-Tsu, C., and Jiun-Chuan, L.: Supply and removal of sediment in a landslide-dominated mountain belt: Central Range, Taiwan, Journal of Geology, 108, 73–89, https://doi.org/10.1086/314387, 2000.

Hua, Q., Turnbull, J. C., Santos, G. M., Rakowski, A. Z., Ancapichún, S., de Pol-Holz, R., Hammer, S., Lehman, S. J., Levin, I., Miller, J. B., Palmer, J. G., and Turney, C. S. M.: Atmospheric radiocarbon for the period 1950-2019, Radiocarbon, 64, 723–745, https://doi.org/10.1017/RDC.2021.95, 2022.

Inamdar, S., Singh, S., Dutta, S., Levia, D., Mitchell, M., Scott, D., Bais, H., and McHale, P.: Fluorescence characteristics and sources of dissolved organic matter for stream water during storm events in a forested mid-Atlantic watershed, J Geophys Res Biogeosci, 116, https://doi.org/10.1029/2011JG001735, 2011.

Inamdar, S., Finger, N., Singh, S., Mitchell, M., Levia, D., Bais, H., Scott, D., and McHale, P.: Dissolved organic matter (DOM) concentration and quality in a forested mid-Atlantic watershed, USA, Biogeochemistry, 108, 55–76, https://doi.org/10.1007/s10533-011-9572-4, 2012.

IPCC: *Climate Change 2021: The Physical Science Basis. Contribution of Working Group I to the Sixth Assessment Report of the Intergovernmental Panel on Climate Change* [Masson-Delmotte, V., P. Zhai, A. Pirani, S.L. Connors, C. Péan, S. Berger, N. Caud, Y. Chen, L. Goldfarb, M.I. Gomis, M. Huang, K. Leitzell, E. Lonnoy, J.B.R. Matthews, T.K. Maycock, T. Waterfield, O. Yelekçi, R. Yu, and B. Zhou (eds.)]. Cambridge University Press, Cambridge, United Kingdom and New York, NY, USA, In press, doi:10.1017/9781009157896, 2021.

Jaun, S. and Ahrens, B.: Evaluation of a probabilistic hydrometeorological forecast system, Hydrology and Earth System Sciences Discussions, 6, 1843–1877, https://doi.org/10.5194/hessd-6-1843-2009, 2009.

Jochner, M., Turowski, J. M., Badoux, A., Stoffel, M., and Rickli, C.: The role of log jams and exceptional flood events in mobilizing coarse particulate organic matter in a steep headwater stream, Earth Surface Dynamics, 3, 311–320, https://doi.org/10.5194/esurf-3-311-2015, 2015.

Kahraman, A., Kendon, E. J., Chan, S. C., and Fowler, H. J.: Quasi-Stationary Intense Rainstorms Spread Across Europe Under Climate Change, Geophys Res Lett, 48, https://doi.org/10.1029/2020GL092361, 2021.

Känel, B., Götz, C., Niederhauser, P., Sinniger, J., and Steinmann, P.: Zustand der Fliessgewässer von Limmat, Sihl und Zürichsee - Messkampagne 2020, 12 pp., 2021.

Kao, S. J. and Liu, K. K.: Stable carbon and nitrogen isotope systematics in a human disturbed watershed (Lanyang-Hsi) in Taiwan and the estimation of biogenic particulate organic carbon and nitrogen fluxes, Global Biogeochem Cycles, 14, 189–198, https://doi.org/10.1029/1999GB900079, 2000.

Karpatne, A., Ebert-Uphoff, I., Ravela, S., Babaie, H. A., and Kumar, V.: Machine Learning for the Geosciences: Challenges and Opportunities, IEEE Trans Knowl Data Eng, 31, 1544–1554, https://doi.org/10.1109/TKDE.2018.2861006, 2019.

Keaveney, E. M. and Reimer, P. J.: Understanding the variability in freshwater radiocarbon reservoir offsets: A cautionary tale, J Archaeol Sci, 39, 1306–1316, https://doi.org/10.1016/j.jas.2011.12.025, 2012.

Keller, H. M. and Weibel, P.: Suspended Sediments in Streamwater - Indicators of Erosion and Bed Load Transport in Mountainous Basins. IAHS Publication No. 203, in: Sediment and Stream Water Quality in a Changing Environment: Trends and Explanation, 53–61, 1991.

Kohn, M. J.: Carbon isotope compositions of terrestrial C3 plants as indicators of (paleo)ecology and (paleo)climate., Proc Natl Acad Sci U S A, 107, 19691–5, https://doi.org/10.1073/pnas.1004933107, 2010.

Komada, T., Druffel, E. R. M., and Trumbore, S. E.: Oceanic export of relict carbon by small mountainous rivers, Geophys Res Lett, 31, https://doi.org/10.1029/2004GL019512, 2004.

Korup, O. and Schlunegger, F.: Rock-type control on erosion-induced uplift, eastern Swiss Alps, Earth Planet Sci Lett, 278, 278–285, https://doi.org/10.1016/j.epsl.2008.12.012, 2009.

Lang, S. Q., Bernasconi, S. M., and Früh-Green, G. L.: Stable isotope analysis of organic carbon in small (μg C) samples and dissolved organic matter using a GasBench preparation device, Rapid Communications in Mass Spectrometry, 26, 9–16, https://doi.org/10.1002/rcm.5287, 2012.

Lang, S. Q., Mcintyre, C. P., Bernasconi, S. M., Früh-Green, G. L., Voss, B. M., Eglinton, T. I., and Wacker, L.: Rapid ^{14}C Analysis of Dissolved Organic Carbon in Non-Saline Waters, Radiocarbon, 58, 1–11, https://doi.org/10.1017/RDC.2016.17, 2016.

Lauerwald, R., Laruelle, G. G., Hartmann, J., Ciais, P., and Regnier, P. A. G.: Spatial patterns in CO_2 evasion from the global river network, Global Biogeochem Cycles, 29, 534–554, https://doi.org/10.1002/2014GB004941, 2015.

Lauerwald, R., Regnier, P., Guenet, B., Friedlingstein, P., and Ciais, P.: How Simulations of the Land Carbon Sink Are Biased by Ignoring Fluvial Carbon Transfers: A Case Study for the Amazon Basin, One Earth, 3, 226–236, https://doi.org/10.1016/j.oneear.2020.07.009, 2020.

LeGrande, A. N. and Schmidt, G. A.: Global gridded data set of the oxygen isotopic composition in seawater, Geophys Res Lett, 33, 1–5, https://doi.org/10.1029/2006GL026011, 2006.

Lehmann, J. and Kleber, M.: The contentious nature of soil organic matter., Nature, 528, 60–8, https://doi.org/10.1038/nature16069, 2015.

Lehmann, M. F., Bernasconi, S. M., Barbieri, A., and Mckenzie, J. A.: Preservation of organic matter and alteration of its carbon and nitrogen isotope composition during simulated and in situ early sedimentary diagenesis, Geochim Cosmochim Acta, 66, 3573–3584, https://doi.org/10.1016/S0016-7037(02)00968-7, 2002.

Lehmann, M. F., Bernasconi, S. M., Barbieri, A., Simona, M., and McKenzie, J. A.: Interannual variation of the isotopic composition of sedimenting organic carbon and nitrogen in Lake Lugano: A long-term sediment trap study, Limnol Oceanogr, 49, 839–849, https://doi.org/10.4319/lo.2004.49.3.0839, 2004.

Leithold, E. L., Blair, N. E., and Perkey, D. W.: Geomorphologic controls on the age of particulate organic carbon from small mountainous and upland rivers, Global Biogeochem Cycles, 20, 1–11, https://doi.org/10.1029/2005GB002677, 2006.

Leithold, E. L., Blair, N. E., and Wegmann, K. W.: Source-to-sink sedimentary systems and global carbon burial: A river runs through it, Earth Sci Rev, 153, 30–42, https://doi.org/10.1016/j.earscirev.2015.10.011, 2016.

Li, M., Peng, C., Zhou, X., Yang, Y., Guo, Y., Shi, G., and Zhu, Q.: Modeling Global Riverine DOC Flux Dynamics From 1951 to 2015, J Adv Model Earth Syst, 11, 514–530, https://doi.org/10.1029/2018MS001363, 2019.

Longworth, B. E., Petsch, S. T., Raymond, P. A., and Bauer, J. E.: Linking lithology and land use to sources of dissolved and particulate organic matter in headwaters of a temperate, passive-margin river system, Geochim Cosmochim Acta, 71, 4233–4250, https://doi.org/10.1016/j.gca.2007.06.056, 2007.

Lyons, W. B., Nezat, C. A., Carey, A. E., and Hicks, D. M.: Organic carbon fluxes to the ocean from high-standing islands, Geology, 30, 443–446, https://doi.org/10.1130/0091-7613(2002)030<0443:OCFTTO>2.0.CO;2, 2002.

Marwick, T. R., Borges, A. V., van Acker, K., Darchambeau, F., and Bouillon, S.: Disproportionate Contribution of Riparian Inputs to Organic Carbon Pools in Freshwater Systems, Ecosystems, 17, 974–989, https://doi.org/10.1007/s10021-014-9772-6, 2014.

Marwick, T. R., Tammoh, F., Teodoru, C. R., Borges, A. v., Darchambeau, F., and Bouillon, S.: The age of river-transported carbon: A global perspective, Global Biogeochem Cycles, 29, 122–137, https://doi.org/10.1002/2014GB004911, 2015.

Masiello, A. and Druffel, E. R. M.: Carbon isotope geochemistry of the Santa Clara River, Global Biogeochem Cycles, 15, 407–416, 2001.

Mayorga, E., Aufdenkampe, A. K., Masiello, C. A., Krusche, A. v., Hedges, J. I., Quay, P. D., Richey, J. E., and Brown, T. A.: Young organic matter as a source of carbon dioxide outgassing from Amazonian rivers, Nature, 436, 538–541, https://doi.org/10.1038/nature03880, 2005.

McCallister, S. L., Bauer, J. E., Cherrier, J. E., and Ducklow, H. W.: Assessing sources and ages of organic matter supporting river and estuarine bacterial production: A multiple-isotope ($\Delta^{14}C$, $\delta^{13}C$, and $\delta^{15}N$) approach, Limnol Oceanogr, 49, 1687–1702, https://doi.org/10.4319/lo.2004.49.5.1687, 2004.

McCulloch, W. S. and Pitts, W.: A logical calculus of the ideas immanent in nervous activity, Bulletin of Mathematical Biophysics, 5, 115–133, https://doi.org/10.1007/978-3-030-01370-7_61, 1943.

McIntyre, C. P., Lechleitner, F., Lang, S. Q., Haghiour, N., Fahrni, S., Wacker, L., and Synal, H. A.: ^{14}C Contamination Testing in Natural Abundance Laboratories: A New Preparation Method Using Wet Chemical Oxidation and Some Experiences, Radiocarbon, 58, 935–941, https://doi.org/10.1017/RDC.2016.78, 2016.

Medeiros, P. M., Sikes, E. L., Thomas, B., and Freeman, K. H.: Flow discharge influences on input and transport of particulate and sedimentary organic carbon along a small temperate river, Geochim Cosmochim Acta, 77, 317–334, https://doi.org/10.1016/j.gca.2011.11.020, 2012.

Milliman, J. D. and Farnsworth, K. L.: River Discharge to the Coastal Ocean. A global synthesis, 2nd ed., Cambridge University Press, Cambridge, New York, Melbourne, Madrid, Cape Town, Singapore, Sao Paulo, Dehli, Tokyo, Mexico City, 384 pp., 2013.

Milliman, J. D. and Syvitski, J. P. M.: Geomorphic/Tectonic Control of Sediment Discharge to the Ocean: The Importance of Small Mountainous Rivers, J Geol, 100, 525–544, https://doi.org/10.1086/629606, 1992.

Milzow, C., Molnar, P., McArdell, B. W., and Burlando, P.: Spatial organization in the step-pool structure of a steep mountain stream (Vogelbach, Switzerland), Water Resour Res, 42, https://doi.org/10.1029/2004WR003870, 2006.

Moore, S., Evans, C. D., Page, S. E., Garnett, M. H., Jones, T. G., Freeman, C., Hooijer, A., Wiltshire, A. J., Limin, S. H., and Gauci, V.: Deep instability of deforested tropical peatlands revealed by fluvial organic carbon fluxes, Nature, 493, 660–663, https://doi.org/10.1038/nature11818, 2013.

Myhre, G., Alterskjær, K., Stjern, C. W., Hodnebrog, Marelle, L., Samset, B. H., Sillmann, J., Schaller, N., Fischer, E., Schulz, M., and Stohl, A.: Frequency of extreme precipitation increases extensively with event rareness under global warming, Sci Rep, 9, https://doi.org/10.1038/s41598-019-52277-4, 2019.

Nussbaum, M., Papritz, A., Baltensweiler, A., and Walthert, L.: Estimating soil organic carbon stocks of Swiss forest soils by robust external-drift kriging, Geosci Model Dev, 7, 1197–1210, https://doi.org/10.5194/gmd-7-1197-2014, 2014.

O'Leary, M. H.: Carbon Isotopes in Photosynthesis, Bioscience, 38, 328–336, https://doi.org/10.2307/1310735, 1988.

Olyaie, E., Banejad, H., Chau, K. W., and Melesse, A. M.: A comparison of various artificial intelligence approaches performance for estimating suspended sediment load of river systems: a case study in United States, Environ Monit Assess, 187, https://doi.org/10.1007/s10661-015-4381-1, 2015.

Peters, W., Bastos, A., Ciais, P., and Vermeulen, A.: A historical, geographical and ecological perspective on the 2018 European summer drought, https://doi.org/10.1098/rstb.2019.0505, 26 October 2020.

Petsch, S. T., Eglinton, T. I., and Edwards, K. J.: ^{14}C-dead living biomass: Evidence for microbial assimilation of ancient organic carbon during shale weathering, Science (1979), 292, 1127–1131, https://doi.org/10.1126/science.1058332, 2001.

Qiao, J., Bao, H., Huang, D., Li, D. W., Lee, T. Y., Huang, J. C., and Kao, S. J.: Runoff-driven export of terrigenous particulate organic matter from a small mountainous river: sources, fluxes and comparisons among different rivers, Biogeochemistry, 147, 71–86, https://doi.org/10.1007/s10533-019-00629-7, 2020.

Raymond, P. A. and Bauer, J. E.: Use of ^{14}C and ^{13}C natural abundances for evaluating riverine, estuarine, and coastal DOC and POC sources and cycling: A review and synthesis, Org Geochem, 32, 469–485, https://doi.org/10.1016/S0146-6380(00)00190-X, 2001.

Raymond, P. A., Bauer, J. E., Caraco, N. F., Cole, J. J., Longworth, B., and Petsch, S. T.: Controls on the variability of organic matter and dissolved inorganic carbon ages in northeast US rivers, Mar Chem, 92, 353–366, https://doi.org/10.1016/j.marchem.2004.06.036, 2004.

Raymond, P. A., Hartmann, J., Lauerwald, R., Sobek, S., McDonald, C., Hoover, M., Butman, D., Striegl, R., Mayorga, E., Humborg, C., Kortelainen, P., Dürr, H., Meybeck, M., Ciais, P., and Guth, P.: Global carbon dioxide emissions from inland waters, Nature, 503, 355–359, https://doi.org/10.1038/nature12760, 2013.

Regnier, P., Friedlingstein, P., Ciais, P., Mackenzie, F. T., Gruber, N., Janssens, I. a., Laruelle, G. G., Lauerwald, R., Luyssaert, S., Andersson, A. J., Arndt, S., Arnosti, C., Borges, A. v., Dale, A. W., Gallego-Sala, A., Goddéris, Y., Goossens, N., Hartmann, J., Heinze, C., Ilyina, T., Joos, F., LaRowe, D. E., Leifeld, J., Meysman, F. J. R., Munhoven, G., Raymond, P. a., Spahni, R., Suntharalingam, P., and Thullner, M.: Anthropogenic perturbation of the carbon fluxes from land to ocean, Nat Geosci, 6, 597–607, https://doi.org/10.1038/ngeo1830, 2013.

Regnier, P., Resplandy, L., Najjar, R. G., and Ciais, P.: The land-to-ocean loops of the global carbon cycle, https://doi.org/10.1038/s41586-021-04339-9, 17 March 2022.

Reichstein, M., Camps-Valls, G., Stevens, B., Jung, M., Denzler, J., Carvalhais, N., and Prabhat: Deep learning and process understanding for data-driven Earth system science, Nature, 566, 195–204, https://doi.org/10.1038/s41586-019-0912-1, 2019.

Reimer, P. J., Brown, T. A., and Reimer, R. W.: Discussion: Reporting and Calibration of Post-Bomb ^{14}C Data, Radiocarbon, 46, 1290–1304, https://doi.org/10.2458/azu_js_rc.46.4183, 2004.

Repasch, M., Scheingross, J. S., Hovius, N., Lupker, M., Wittmann, H., Haghipour, N., Gröcke, D. R., Orfeo, O., Eglinton, T. I., and Sachse, D.: Fluvial organic carbon cycling regulated by sediment transit time and mineral protection, Nat Geosci, 14, 842–848, https://doi.org/10.1038/s41561-021-00845-7, 2021.

Rickenmann, D., Turowski, J. M., Fritschi, B., Klaiber, A., and Ludwig, A.: Bedload transport measurements at the Erlenbach stream with geophones and automated basket samplers, Earth Surf Process Landf, 37, 1000–1011, https://doi.org/10.1002/esp.3225, 2012.

Romaní, A. M., Guasch, H., Muñoz, I., Ruana, J., Vilalta, E., Schwartz, T., Emtiazi, F., and Sabater, S.: Biofilm structure and function and possible implications for riverine DOC dynamics, Microb Ecol, 47, 316–328, https://doi.org/10.1007/s00248-003-2019-2, 2004.

Rowland, R., Inamdar, S., and Parr, T.: Evolution of particulate organic matter (POM) along a headwater drainage: role of sources, particle size class, and storm magnitude, Biogeochemistry, 133, 181–200, https://doi.org/10.1007/s10533-017-0325-x, 2017.

Ruiz-Villanueva, V., Mazzorana, B., Bladé, E., Bürkli, L., Iribarren-Anacona, P., Mao, L., Nakamura, F., Ravazzolo, D., Rickenmann, D., Sanz-Ramos, M., Stoffel, M., and Wohl, E.: Characterization of wood-laden flows in rivers, Earth Surf Process Landf, 44, 1694–1709, https://doi.org/10.1002/esp.4603, 2019.

Rumelhart, D. E., Hinton, G. E., and Williams, R. J.: Learning representations by back-propagating errors, Nature, 323, 533–5.36, 1986.

Scheingross, J. S., Hovius, N., Dellinger, M., Hilton, R. G., Repasch, M., Sachse, D., Gröcke, D. R., Vieth-Hillebrand, A., and Turowski, J. M.: Preservation of organic carbon during active fluvial transport and particle abrasion, Geology, 47, 958–962, https://doi.org/10.1130/G46442.1, 2019.

Scheingross, J. S., Repasch, M. N., Hovius, N., Sachse, D., Lupker, M., Fuchs, M., Halevy, I., Gröcke, D. R., Golombek, N. Y., Haghipour, N., Eglinton, T. I., Orfeo, O., and Schleicher, A. M.: The fate of fluvially-deposited organic carbon during transient floodplain storage, Earth Planet Sci Lett, 561, https://doi.org/10.1016/j.epsl.2021.116822, 2021.

Schleppi, P., Muller, N., Feyen, H., Papritz, A., Bucher, J. B. J. B., Fliihler, H., and Flühler, H.: Nitrogen budgets of two small experimental forested catchments at Alptal, Switzerland, For Ecol Manage, 101, 177–185, https://doi.org/10.1016/S0378-1127(97)00134-5, 1998.

Schleppi, P., Waldner, P. A., and Fritschi, B.: Accuracy and precision of different sampling strategies and flux integration methods for runoff water: Comparisons based on measurements of the electrical conductivity, Hydrol Process, 20, 395–410, https://doi.org/10.1002/hyp.6057, 2006.

Schmidt, S., Alewell, C., Panagos, P., and Meusburger, K.: Regionalization of monthly rainfall erosivity patternsin Switzerland, Hydrol Earth Syst Sci, 20, 4359–4373, https://doi.org/10.5194/hess-20-4359-2016, 2016.

Schmidt, S., Alewell, C., and Meusburger, K.: Monthly RUSLE soil erosion risk of Swiss grasslands, J Maps, 15, 247–256, https://doi.org/10.1080/17445647.2019.1585980, 2019.

Schuerch, P., Densmore, A. L., McArdell, B. W., and Molnar, P.: The influence of landsliding on sediment supply and channel change in a steep mountain catchment, Geomorphology, 78, 222–235, https://doi.org/10.1016/j.geomorph.2006.01.025, 2006.

Schuwirth, N., Kühni, M., Schweizer, S., Uehlinger, U., and Reichert, P.: A mechanistic model of benthos community dynamics in the River Sihl, Switzerland, Freshw Biol, 53, 1372–1392, https://doi.org/10.1111/j.1365-2427.2008.01970.x, 2008.

Schwab, M. S., Hilton, R. G., Haghipour, N., Baronas, J. J., and Eglinton, T. I.: Vegetal Undercurrents—Obscured Riverine Dynamics of Plant Debris, J Geophys Res Biogeosci, 127, https://doi.org/10.1029/2021jg006726, 2022.

Schwab, M. S., and Gies, H.: Subalpine Sihl River Time-Series: Particulate and Dissolved Organic Carbon contents and Isotopic Compositions, Version 1.0. Interdisciplinary Earth Data Alliance (IEDA). https://doi.org/10.26022/IEDA/112503, 2022.

Sharafati, A., Haji Seyed Asadollah, S. B., Motta, D., and Yaseen, Z. M.: Application of newly developed ensemble machine learning models for daily suspended sediment load prediction and related uncertainty analysis, Hydrological Sciences Journal, 2022–2042, https://doi.org/10.1080/02626667.2020.1786571, 2020.

Smith, J. C., Galy, A., Hovius, N., Tye, A. M., Turowski, J. M., and Schleppi, P.: Runoff-driven export of particulate organic carbon from soil in temperate forested uplands, Earth Planet Sci Lett, 365, 198–208, https://doi.org/10.1016/j.epsl.2013.01.027, 2013.

Spencer, R. G. M., Guo, W., Raymond, P. A., Dittmar, T., Hood, E., Fellman, J., and Stubbins, A.: Source and biolability of ancient dissolved organic matter in glacier and lake ecosystems on the Tibetan plateau, Geochim Cosmochim Acta, 142, 64–74, https://doi.org/10.1016/j.gca.2014.08.006, 2014.

Spreafico, M.: Environmental impact caused by reservoir sedimentation management Advanced Training Workshop on Reservoir Sedimentation Management, 10-16 October 2007, Beijing China, 2007.

Spreafico, M., Lehmann, Ch., Jakob, A., and Grasso, A.: Feststoffbeobachtung in der Schweiz, 101 pp., 2005.

Srivastava, N., Hinton, G., Krizhevsky, A., and Salakhutdinov, R.: Dropout: A Simple Way to Prevent Neural Networks from Overfitting, Journal of Machine Learning Research, 1929–1958 pp., 2014.

Stock, B. C. and Semmens, B. X.: MixSIAR GUI User Manual. Version 3.1., https://doi.org/doi:10.5281/zenodo.1209993, 2016.

Stock, B. C., Jackson, A. L., Ward, E. J., Parnell, A. C., Phillips, D. L., and Semmens, B. X.: Analyzing mixing systems using a new generation of Bayesian tracer mixing models, PeerJ, 6:e5096, https://doi.org/10.7717/peerj.5096, 2018.

Stubbins, A., Hood, E., Raymond, P. A., Aiken, G. R., Sleighter, R. L., Hernes, P. J., Butman, D., Hatcher, P. G., Striegl, R. G., Schuster, P., Abdulla, H. A. N., Vermilyea, A. W., Scott, D. T., and Spencer, R. G. M.: Anthropogenic aerosols as a source of ancient dissolved organic matter in glaciers, Nat Geosci, 5, 198–201, https://doi.org/10.1038/ngeo1403, 2012.

Sutfin, N. A., Wohl, E. E., and Dwire, K. A.: Banking carbon: A review of organic carbon storage and physical factors influencing retention in floodplains and riparian ecosystems, Earth Surf Process Landf, 41, 38–60, https://doi.org/10.1002/esp.3857, 2016.

Syvitski, J. P., Morehead, M. D., Bahr, D. B., and Mulder, T.: Estimating fluvial sediment transport: The rating parameters, Water Resour Res, 36, 2747–2760, https://doi.org/10.1029/2000WR900133, 2000.

Talbot, C. J., Bennett, E. M., Cassell, K., Hanes, D. M., Minor, E. C., Paerl, H., Raymond, P. A., Vargas, R., Vidon, P. G., Wollheim, W., and Xenopoulos, M. A.: The impact of flooding on aquatic ecosystem services, Biogeochemistry, 141, 439–461, https://doi.org/10.1007/s10533-018-0449-7, 2018.

Tranvik, L. J., Downing, J. A., Cotner, J. B., Loiselle, S. A., Striegl, R. G., Ballatore, T. J., Dillon, P., Finlay, K., Fortino, K., Knoll, L. B., Kortelainen, P. L., Kutser, T., Larsen, S., Laurion, I., Leech, D. M., Leigh McCallister, S., McKnight, D. M., Melack, J. M., Overholt, E., Porter, J. A., Prairie, Y., Renwick, W. H., Roland, F., Sherman, B. S., Schindler, D. W., Sobek, S., Tremblay, A., Vanni, M. J., Verschoor, A. M., von Wachenfeldt, E., and Weyhenmeyer, G. A.: Lakes and reservoirs as regulators of carbon cycling and climate, Limnol Oceanogr, 54, 2298–2314, https://doi.org/10.4319/lo.2009.54.6_part_2.2298, 2009.

Turowski, J. M., Yager, E. M., Badoux, A., Rickenmann, D., and Molnar, P.: The impact of exceptional events on erosion, bedload transport and channel stability in a step-pool channel, Earth Surf Process Landf, 34, 613–628, https://doi.org/10.1002/esp, 2009.

Turowski, J. M., Badoux, A., and Rickenmann, D.: Start and end of bedload transport in gravel-bed streams, Geophys Res Lett, 38, 1–5, https://doi.org/10.1029/2010GL046558, 2011.

Turowski, J. M., Badoux, A., Bunte, K., Rickli, C., Federspiel, N., and Jochner, M.: The mass distribution of coarse particulate organic matter exported from an Alpine headwater stream, Earth Surface Dynamics, 1, 1–11, https://doi.org/10.5194/esurf-1-1-2013, 2013.

Turowski, J. M., Hilton, R. G., and Sparkes, R.: Decadal carbon discharge by a mountain stream is dominated by coarse organic matter, Geology, 44, 27–30, https://doi.org/10.1130/G37192.1, 2016.

Upadhayay, H. R., Bodé, S., Griepentrog, M., Huygens, D., Bajracharya, R. M., Blake, W. H., Dercon, G., Mabit, L., Gibbs, M., Semmens, B. X., Stock, B. C., Cornelis, W., and Boeckx, P.: Methodological perspectives on the application of compound-specific stable isotope fingerprinting for sediment source apportionment, https://doi.org/10.1007/s11368-017-1706-4, 1 June 2017.

van der Voort, T. S., Hagedorn, F., McIntyre, C., Zell, C., Walthert, L., Schleppi, P., Feng, X., and Eglinton, T. I.: Variability in ^{14}C contents of soil organic matter at the plot and regional scale across climatic and geologic gradients, Biogeosciences, 13, 3427–3439, https://doi.org/10.5194/bg-13-3427-2016, 2016.

van der Voort, T. S. van der, Mannu, U., Hagedorn, F., McIntyre, C. P., Walthert, L., Schleppi, P., Haghipour, N., and Eglinton, T. I.: Dynamics of deep soil carbon - insights from ^{14}C time series across a climatic gradient, Biogeosciences, 16, 3233–3246, https://doi.org/10.5194/bg-16-3233-2019, 2019.

von Wachenfeldt, E. and Tranvik, L. J.: Sedimentation in boreal lakes - The role of flocculation of allochthonous dissolved organic matter in the water column, Ecosystems, 11, 803–814, https://doi.org/10.1007/s10021-008-9162-z, 2008.

Wacker, L., Bonani, G., Friedrich, M., Hajdas, I., Kromer, B., Nemec, M., Ruff, M., Suter, M., Synal, H., and Vockenhuber, C.: MICADAS: Routine and High-Precision Radiocarbon Dating, Radiocarbon, 52, 252–262, https://doi.org/10.2458/azu_js_rc.52.3660, 2010.

Walling, D. E.: Assessing the accuracy of suspended sediment rating curves for a small basin, Water Resour Res, 13, 531–538, https://doi.org/10.1029/WR013i003p00531, 1977.

Wang, G., Jia, Y., and Li, W.: Effects of environmental and biotic factors on carbon isotopic fractionation during decomposition of soil organic matter, Sci Rep, 5, https://doi.org/10.1038/srep11043, 2015.

Wang, J., Jin, Z., Hilton, R. G., Zhang, F., Li, G., Densmore, A. L., Gröcke, D. R., Xu, X., and Joshua West, A.: Earthquake-triggered increase in biospheric carbon export from a mountain belt, Geology, 44, 471–474, https://doi.org/10.1130/G37533.1, 2016.

Waser, L. T., Ginzler, C., and Rehush, N.: Wall-to-Wall tree type mapping from countrywide airborne remote sensing surveys, Remote Sens (Basel), 9, https://doi.org/10.3390/rs9080766, 2017.

Werth, M. and Kuzyakov, Y.: ^{13}C fractionation at the root-microorganisms-soil interface: A review and outlook for partitioning studies, https://doi.org/10.1016/j.soilbio.2010.04.009, September 2010.

West, A. J., Lin, C. W., Lin, T. C., Hilton, R. G., Liu, S. H., Chang, C. T., Lin, K. C., Galy, A., Sparkes, R. B., and Hovius, N.: Mobilization and transport of coarse woody debris to the oceans triggered by an extreme tropical storm, Limnol Oceanogr, 56, 77–85, https://doi.org/10.4319/lo.2011.56.1.0077, 2011.

Wheatcroft, R. A., Goñi, M. A., Hatten, J. A., Pasternack, G. B., and Warrick, J. A.: The role of effective discharge in the ocean delivery of particulate organic carbon by small, mountainous river systems, Limnol Oceanogr, 55, 161–171, https://doi.org/10.4319/lo.2010.55.1.0161, 2010.

Winkler, W., Wildi, W., van Stuijvenberg, J., and Caron, C.: Wägital-Flysch et autres flyschs jenniques en Suisse Centrale. Stratigraphie, sédimentologie et comparaisons, Eclogae Geologicae Helvetiae, 7, 1–22, 1985.

Wohl, E.: Bridging the gaps: An overview of wood across time and space in diverse rivers, Geomorphology, 279, 3–26, https://doi.org/10.1016/j.geomorph.2016.04.014, 2017.

Wohl, E. and Ogden, F. L.: Organic carbon export in the form of wood during an extreme tropical storm, Upper Rio Chagres, Panama, Earth Surf Process Landf, 38, 1407–1416, https://doi.org/10.1002/esp.3389, 2013.

Wohl, E., Dwire, K., Sutfin, N., Polvi, L., and Bazan, R.: Mechanisms of carbon storage in mountainous headwater rivers, Nat Commun, 3, 1–8, https://doi.org/10.1038/ncomms2274, 2012.

Wymore, A. S., Leon, M. C., Shanley, J. B., and McDowell, W. H.: Hysteretic response of solutes and turbidity at the event scale across forested tropical montane watersheds, Front Earth Sci (Lausanne), 7, https://doi.org/10.3389/feart.2019.00126, 2019.

Zou, H. and Hastie, T.: Regularization and variable selection via the elastic net, J R Stat Soc Series B Stat Methodol, 67, 301–320, https://doi.org/10.1111/j.1467-9868.2005.00503.x, 2005.

Table 1: Summary of river and watershed characteristics for the Sihl River, Erlenbach, Lümpenbach, and Vogelbach streams. Information for the Sihl River headwaters is provided by Smith et al. (2013) and von Freyberg et al. (2018).

		Erlenbach	Lümpenbach	Vogelbach	Sihl - Sihlhölzli
Basin size at gauging station (km^2)[a]		0.73	0.88	1.58	346.02
Average slope (°)[a]		23.9	19.6	28.9	19.5
Mean catchment elevation (m a.s.l.)[a]		1359	1336	1335	1041
Average discharge ($m^3 s^{-1}$)[a]		0.04	0.05	0.07	6.83
Basin geology[b]		Eocene flysch, Cretaceous flysch	Cretaceous flysch	Cretaceous flysch	Subalpine molasse, flysch, limestone, evaporites, sandstone
Land-use[c]	Settlements (%)	0	0	0	9.0
	Agriculture (%)	0	0	0	1.1
	Meadows, pastures (%)	21.6	81	30	38.9
	Forest (%)	59.5	19	70	43.4
	Water bodies (%)	0	0	0	1.3
	Unproductive areas (%)	18.9	0	0	6.1

[a] Federal Office for the Environment, https://www.bafu.admin.ch/bafu/de/home.html
[b] Federal Office of Topography swisstopo, https://www.swisstopo.admin.ch/
[c] Federal Statistic Office, https://www.bfs.admin.ch/bfs/en/home.html

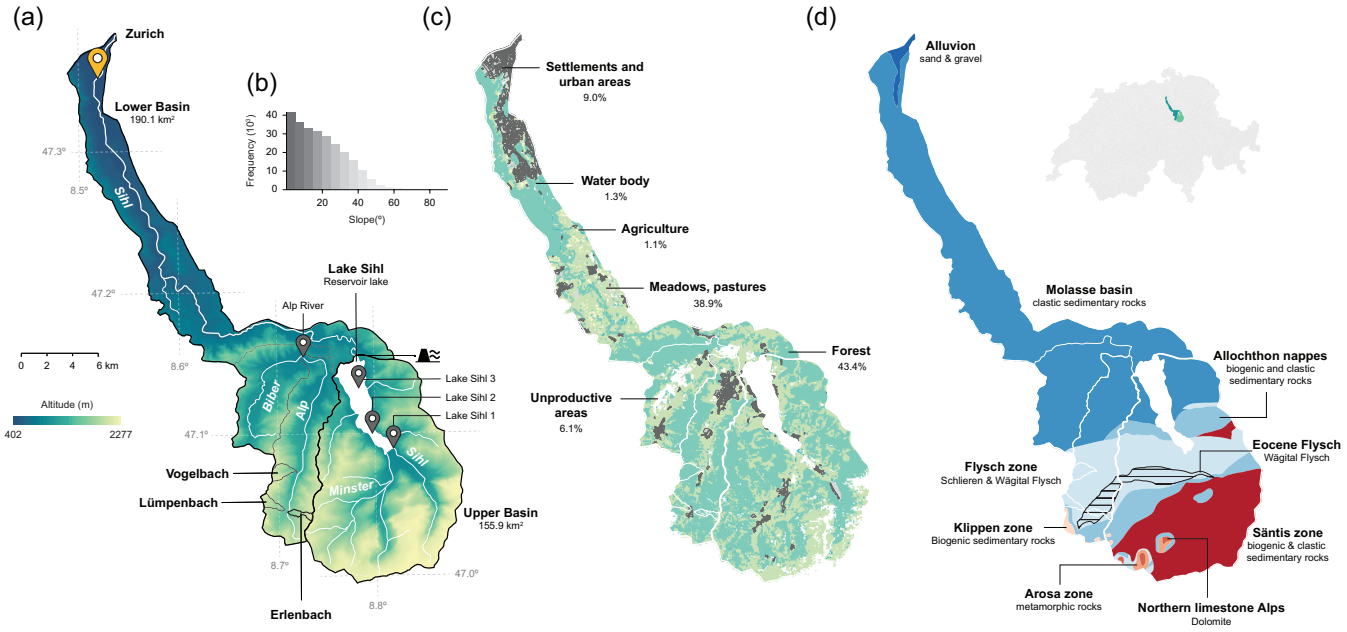

Figure 1: Sihl River basin showing (a) altitude, (b) the distribution of slope angles (https:www.swisstopo.admin.ch), (c) different land-use types (https://www.bfs.admin.ch), and (d) the underlying geology (https:www.swisstopo.admin.ch, Winkler et al., 1985). The sampling location for the Sihl River time series is indicated as a yellow symbol; the locations of the Lake Sihl and the Alp River sampling sites are shown as grey symbols.

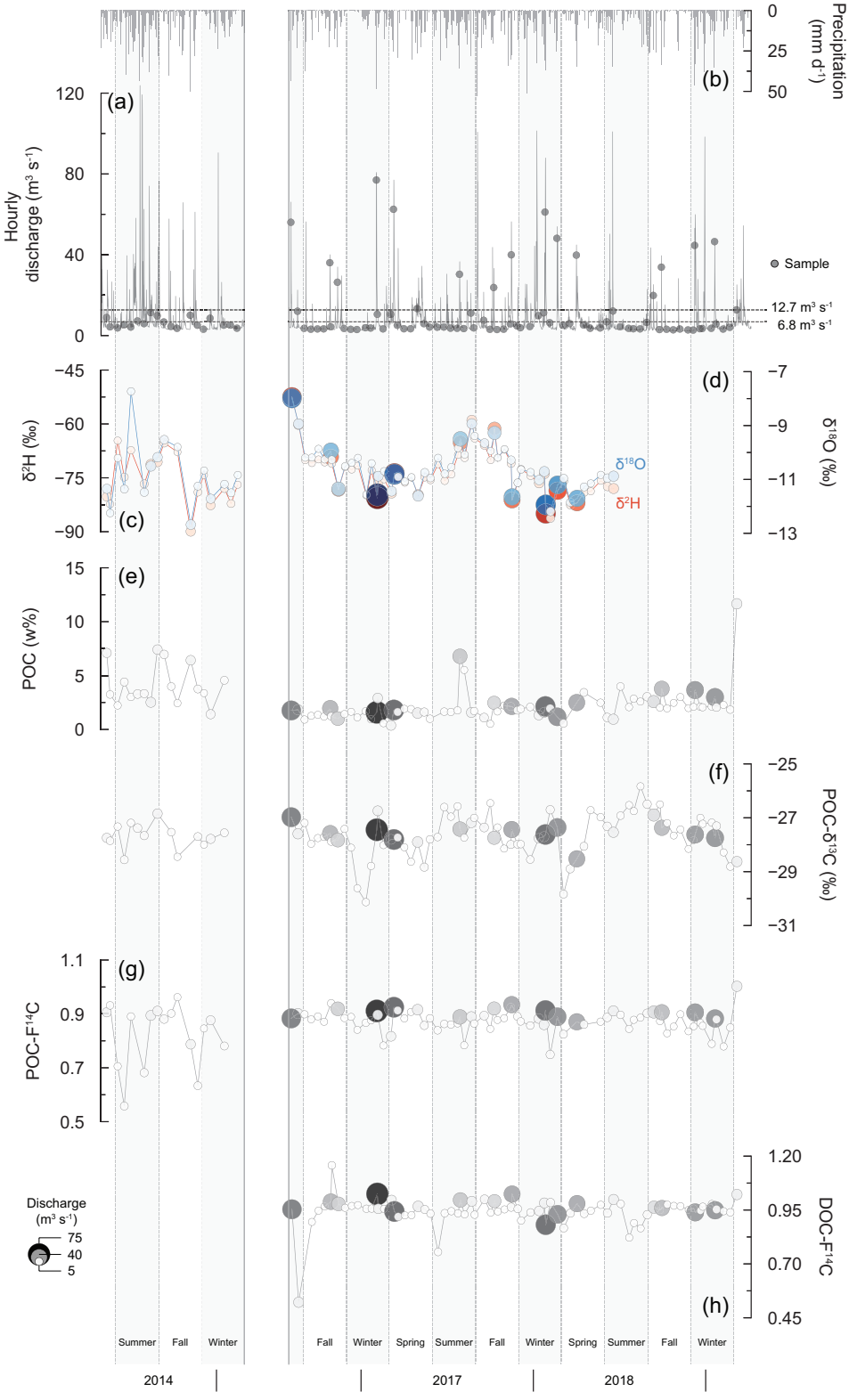
(a)
(b)
(c)
(d)
(e)
(f)
(g)
(h)
Hourly discharge (m³ s⁻¹)
Precipitation (mm d⁻¹)
Sample
12.7 m³ s⁻¹
6.8 m³ s⁻¹
δ²H (‰)
δ¹⁸O (‰)
δ¹⁸O
δ²H
POC (w%)
POC-δ¹³C (‰)
POC-F¹⁴C
DOC-F¹⁴C
Discharge (m³ s⁻¹)
75
40
5
Summer
Fall
Winter
Spring
2014
2017
2018

Figure 2: Hydrographs for the sampling periods from May 2014 to February 2015 and August 2016 to March 2019: (a) hourly discharge values (m^3 s^{-1}; https://www.hydrodaten.admin.ch) and (b) daily precipitation values for the Sihl River basin (mm d^{-1}; https://gate.meteoswiss.ch). Gray dots represent individual sampling campaigns. Water isotopic compositions, (c) δ^2H (‰) and (d) $\delta^{18}O$ (‰), are shown alongside (e) particulate organic carbon (POC) contents (wt%), (f) POC-$\delta^{13}C$ (‰,), (g) POC-$F^{14}C$, and (h) dissolved organic carbon (DOC) $F^{14}C$. Dots are scaled to discharge.

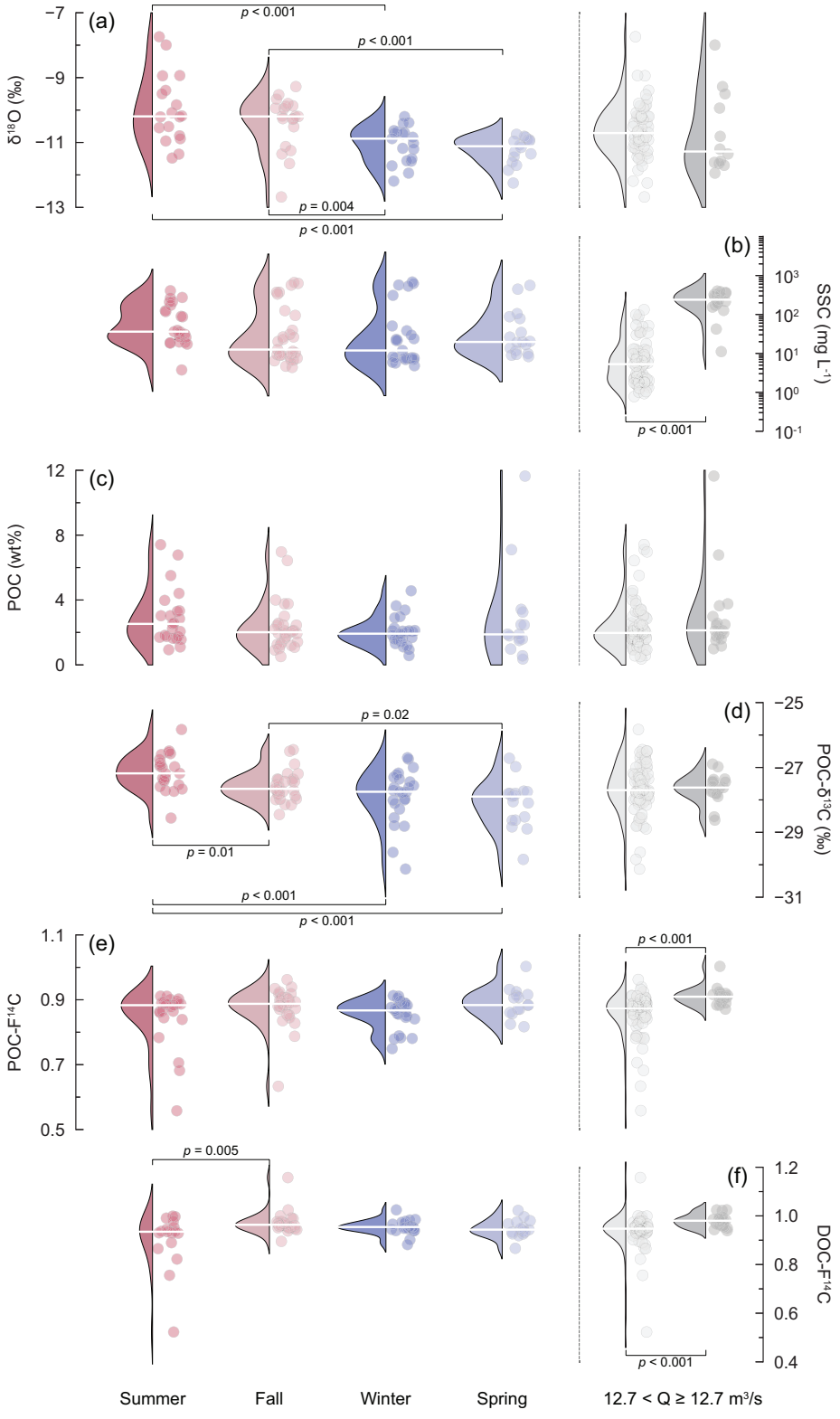
(a)
δ18O (‰)
−7
−9
−11
−13
p < 0.001
p < 0.001
p = 0.004
p < 0.001
(b)
SSC (mg L-1)
10³
10²
10¹
10⁰
10-1
p < 0.001
(c)
POC (wt%)
12
8
4
0
(d)
POC-δ13C (‰)
−25
−27
−29
−31
p = 0.02
p = 0.01
p < 0.001
p < 0.001
(e)
POC-F14C
1.1
0.9
0.7
0.5
p < 0.001
p = 0.005
(f)
DOC-F14C
1.2
1.0
0.8
0.6
0.4
p < 0.001
Summer
Fall
Winter
Spring
12.7 < Q ≥ 12.7 m³/s

Figure 3: Combined violin and strip plots of (a) $\delta^{18}O$ (‰), (b) suspended sediment concentrations (SSC, mg L^{-1}), (c) particulate organic carbon (POC) content (wt%), (d) POC-$\delta^{13}C$ (‰), (e) POC-$F^{14}C$, and (f) dissolved organic carbon (DOC) $F^{14}C$ faceted for seasons and discharge. Violin plots depict rotated kernel density plots. White vertical lines indicate median values. Significant between-group differences are denoted with brackets and *p*-values (**Table E1**).

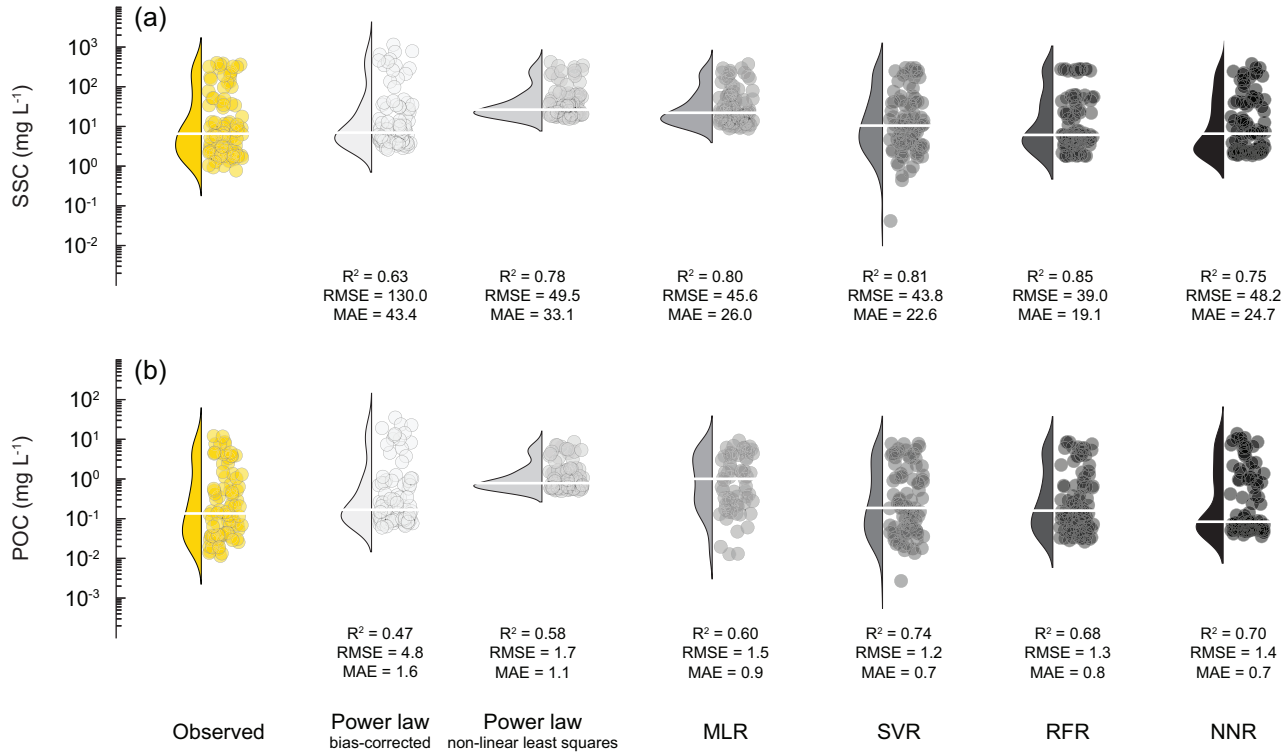

Figure 4: Combined violin and strip plots comparing model performances in predicting (a) suspended sediment (SSC, mg L^{-1}) and (b) particulate organic carbon (POC, mg L^{-1}) concentrations. Models approaches include traditional and non-linear least squares power law functions as well as multilinear regression (MLR), support vector regression (SVR), random forest regression (RFR), and neural network regression (NNR). Violin plots depict rotated kernel density plots, with white horizontal lines indicating median values.

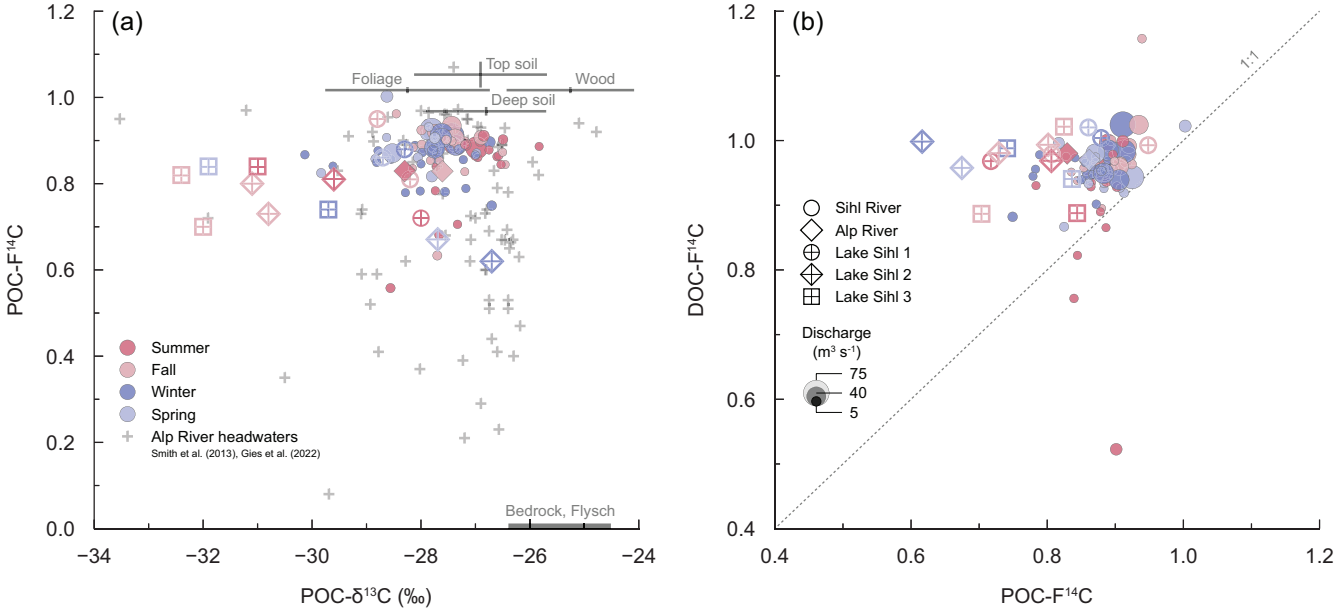

Figure 5: Relationship between (a) particulate organic carbon (POC) $F^{14}C$ and POC-$\delta^{13}C$ (‰) values and (b) between dissolved organic carbon (DOC) and POC-$F^{14}C$ values. Gray crosses indicate samples from the Alptal headwater streams: Erlenbach, Lümpenbach, and Vogelbach (Smith et al., 2013; Gies et al., 2022). Mean isotopic compositions (±SD) of bedrock, foliage, wood, top and deep soil endmembers are depicted. Dots are color-coded for seasons and scaled to discharge.

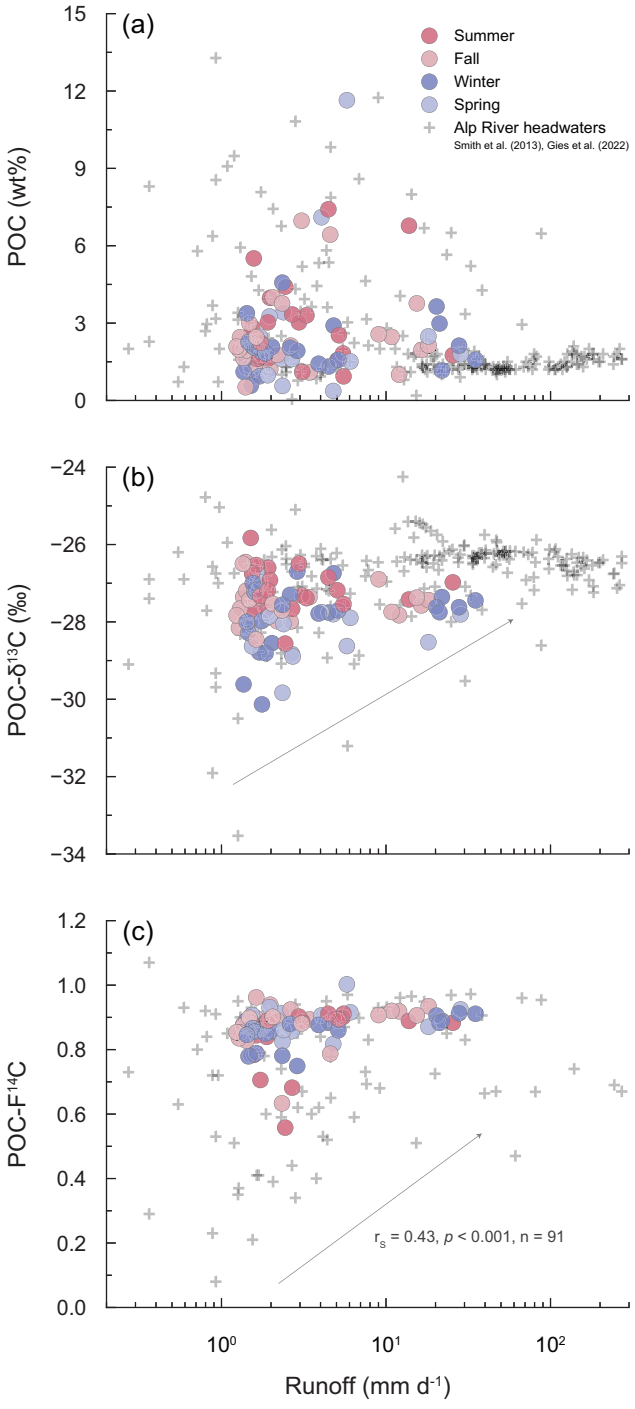

Figure 6: Relationship between runoff (mm d^{-1}), (a) particulate organic carbon (POC) content (wt%), (b) POC-$\delta^{13}C$ (‰), and (c) POC-$F^{14}C$. Gray crosses indicate samples from the Erlenbach, Lümpenbach, and Vogelbach (Smith et al., 2013; Gies et al., 2022). Circles are color-coded for seasons. Gray arrows indicate trends.

Table B1: Particular organic carbon (POC) endmember compositions used in the MixSIAR Bayesian model.

	POC-$\delta^{13}C$ (‰)		POC-$F^{14}C$			Reference
	M	SD	M	SD	n	
Bedrock	-25.45	0.89	0.000	0.001	22	Smith et al. (2013)
Top soil	-26.91	1.20	1.053	0.027	22	Smith et al. (2013); van der Voort et al. (2016); Gies et al. (2022)
Deep soil	-26.80	1.08	0.968	0.007	5	Smith et al. (2013); van der Voort et al. (2016); Gies et al. (2022)
Foliage	-28.25	1.49	1.017	0.004	8	Smith et al. (2013); Hua et al. (2022)
Wood	-25.26	1.15	1.017	0.004	12	Smith et al. (2013); Hua et al. (2022)

Table C1: Model performance in predicting suspended sediment (SS) and particulate organic carbon (POC) concentrations for the investigated period. SS: suspended sediment, POC: particulate organic carbon, Q: discharge, H: water stage, P: precipitation, P_{t-1}: 1-day antecedent precipitation, P_{t-2}: 2-day antecedent precipitation.

Model	Scenario	Model structure	R^2	RMSE	MAE	R^2	RMSE	MAE
				mg L^{-1}	mg L^{-1}		mg L^{-1}	mg L^{-1}
Suspended Sediment Concentration								
Power Law (biased corrected)						*Power Law (non-linear least squares)*		
			0.628	130.027	43.355	0.777	49.534	33.086
Multiple Linear Regression (Elastic Net)						*Random Forest Regression*		
	1	SS ~ Q	0.769	48.241	26.720	0.831	41.617	20.951
	2	SS ~ Q + H	0.781	47.119	26.052	0.789	47.633	24.752
	3	SS ~ Q + H + P	0.775	47.877	26.440	0.809	46.130	23.236
	4	SS ~ Q + H + P + P_{t-1}	0.791	46.171	26.236	0.829	41.131	20.961
	5	SS ~ Q + H + P + P_{t-1} + P_{t-2}	0.791	46.165	26.597	0.823	44.162	21.384
	6	SS ~ P_{t-1}	0.530	66.768	40.194	0.589	67.226	28.772
	7	SS ~ P_{t-1} + Q	0.792	45.974	**25.824**	**0.847**	**39.027**	**19.136**
	8	SS ~ P_{t-1} + Q + H	**0.796**	**45.568**	26.007	0.783	41.032	20.784
	9	SS ~ H	0.673	57.444	34.489	0.670	56.707	32.647
	10	SS ~ H + P_{t-1}	0.666	57.614	35.160	0.659	54.453	27.061
	11	SS ~ P	0.335	81.021	56.256	0.115	99.313	58.731
Support Vector Regression						*Neural Network Regression*		
	1	SS ~ Q	0.796	45.110	23.504	0.717	50.760	27.259
	2	SS ~ Q + H	**0.810**	**43.846**	22.647	**0.752**	**48.235**	24.726
	3	SS ~ Q + H + P	0.751	50.146	25.362	0.746	48.390	25.518
	4	SS ~ Q + H + P + P_{t-1}	0.771	48.357	22.429	0.728	48.316	**24.640**
	5	SS ~ Q + H + P + P_{t-1} + P_{t-2}	0.763	48.937	23.132	0.734	48.845	25.634
	6	SS ~ P_{t-1}	0.358	79.794	37.551	0.435	71.182	32.648
	7	SS ~ P_{t-1} + Q	0.793	45.320	21.168	0.690	49.812	25.873
	8	SS ~ P_{t-1} + Q + H	0.799	44.745	**20.701**	0.741	49.391	25.241
	9	SS ~ H	0.479	70.756	34.971	0.593	59.417	28.658
	10	SS ~ H + P_{t-1}	0.604	62.900	29.319	0.669	56.086	27.110
	11	SS ~ P	0.168	91.156	47.051	0.023	97.894	52.224
Particulate Organic Carbon Concentration								
Power Law (biased corrected)						*Power Law (non-linear least squares)*		
			0.474	4.755	1.568	0.584	1.678	1.069
Multiple Linear Regression (Elastic Net)						*Random Forest Regression*		
	1	POC ~ Q	0.362	1.780	1.079	0.467	1.569	0.874
	2	POC ~ Q + H	0.555	1.506	0.841	0.663	1.383	0.765
	3	POC ~ Q + H + P	0.440	1.676	0.974	0.613	1.356	0.780
	4	POC ~ Q + H + P + P_{t-1}	0.592	1.499	0.884	0.642	1.381	0.784
	5	POC ~ Q + H + P + P_{t-1} + P_{t-2}	0.578	1.526	0.913	0.601	1.518	0.847
	6	POC ~ P_{t-1}	0.368	1.757	1.197	0.628	1.598	0.781
	7	POC ~ P_{t-1} + Q	0.464	1.660	0.987	0.503	1.487	0.866
	8	POC ~ P_{t-1} + Q + H	**0.595**	**1.485**	0.871	**0.680**	**1.327**	**0.749**
	9	POC ~ H	0.553	1.509	**0.839**	0.479	1.522	0.864
	10	POC ~ H + P_{t-1}	0.515	1.601	0.999	0.638	1.503	0.747
	11	POC ~ P	0.078	2.006	1.452	-0.263	2.218	1.534
Support Vector Regression						*Neural Network Regression*		
	1	POC ~ Q	0.064	2.061	1.144	0.627	1.471	0.792
	2	POC ~ Q + H	0.636	1.422	0.791	0.579	1.599	0.817
	3	POC ~ Q + H + P	0.663	1.343	0.729	0.574	1.411	0.760
	4	POC ~ Q + H + P + P_{t-1}	**0.735**	**1.226**	**0.670**	0.650	1.479	0.743
	5	POC ~ Q + H + P + P_{t-1} + P_{t-2}	0.594	1.531	0.862	0.285	1.762	0.840

6	POC ~ P_{t-1}	0.498	1.648	0.848	0.590	1.699	0.887
7	POC ~ P_{t-1} + Q	0.531	1.541	0.797	0.667	1.432	0.779
8	POC ~ P_{t-1} + Q + H	0.612	1.455	0.762	0.656	1.468	0.781
9	POC ~ H	0.541	1.579	0.748	0.599	1.466	0.713
10	POC ~ H + P_{t-1}	0.471	1.598	0.792	**0.697**	**1.392**	**0.701**
11	POC ~ P	-0.022	2.305	1.245	0.188	2.250	1.168

Table C2: Modelled export of suspended sediment and particulate organic carbon using traditional and machine learning approaches, averaged over 47 yr (1974-2020 inclusive).

		Mean annual flux (t)					
		Q < 12.7 $m^3 s^{-1}$	Q > 12.7 $m^3 s^{-1}$	Summer	Fall	Winter	Spring
Suspended Sediment							
Power Law (bias-corrected)	25,788.18±3,775.68	1,816.35±48.17 (7.04 %)	23,971.83±3,765.95 (92.96 %)	12,498.98±3,055.68 (48.47 %)	3,373.31±615.71 (13.08 %)	3,100.66±500.32 (12.02 %)	6,815.23±2,343.25 (26.43 %)
Power Law (non-linear least squares)	17,789.77±1,041.51	4,821.24±91.88 (27.10 %)	12,968.53±1,009.22 (72.90 %)	6,502.93±748.95 (36.55 %)	3,061.53±357.74 (17.21 %)	3,023.15±295.25 (16.99 %)	5,202.16±716.82 (29.24 %)
Multiple Linear Regression (Elastic Net)	25,455.62±1,595.16	5,885.17±146.12 (23.12 %)	19,570.46±1,534.49 (76.88 %)	9,550.15±1,140.49 (37.52 %)	4,241.03±551.88 (16.66 %)	4,174.50±453.24 (16.40 %)	7,489.94±1,092.33 (29.42 %)
Support Vector Regression	19,673.18±842.56	4,055.42±127.67 (20.61 %)	15,617.76±763.59 (79.39 %)	6,337.29±535.88 (32.21 %)	3,557.99±3,557.99 (18.09 %)	3,603.13±362.26 (18.31 %)	6,174.77±562.59 (31.39 %)
Random Forest Regression	25,166.54±1,055.81	5,675.07±193.27 (22.55 %)	19,491.48±931.47 (77.45 %)	8,151.50±627.60 (32.39 %)	4,618.15±522.81 (18.35 %)	4,514.11±431.31 (17.94 %)	7,882.78±752.69 (31.32 %)
Neural Network Regression	24,854.07±1,741.07	3,841.13±118.92 (15.45 %)	21,012.94±1,689.47 (84.55 %)	9,651.12±1,260.24 (38.83 %)	4,013.30±576.11 (16.15 %)	3,900.18±478.11 (15.69 %)	7,289.47±1,194.11 (29.33 %)
Particulate Organic Carbon							
Power Law (bias-corrected)	762.68±121.06	45.47±1.24 (5.96 %)	717.21±120.82 (94.04 %)	379.06±98.69 (49.70 %)	96.21±18.21 (12.61 %)	87.57±14.70 (11.48 %)	199.84±74.24 (26.20 %)
Power Law (non-linear least squares)	426.30±21.39	136.13±2.42 (31.93 %)	290.17±20.46 (68.07 %)	148.80±14.94 (34.90 %)	75.80±8.07 (17.78 %)	75.42±6.63 (17.69 %)	126.29±14.84 (29.62 %)
Multiple Linear Regression (Elastic Net)	638.48±33.50	200.05±5.52 (31.33 %)	438.44±30.37 (68.67 %)	227.97±22.17 (35.71 %)	109.50±13.67 (17.15 %)	108.35±10.94 (16.97 %)	192.66±22.42 (30.17 %)
Support Vector Regression	573.48±24.59	156.04±4.89 (27.21 %)	417.44±21.36 (72.79 %)	187.97±14.85 (32.78 %)	104.64±12.58 (18.25 %)	100.16±9.29 (17.46 %)	180.70±17.00 (31.51%)
Random Forest Regression	539.98±21.56	183.60±5.70 (34.00 %)	356.38±17.61 (66.00 %)	167.94±12.25 (31.10 %)	98.29±10.62 (18.20 %)	98.39±8.60 (18.22 %)	175.36±15.03 (32.48%)
Neural Network Regression	580.23±32.64	136.21±4.30 (23.48 %)	444.01±30.25 (76.52 %)	209.88±22.26 (36.17 %)	97.41±12.92 (16.79 %)	95.15±10.37 (16.40 %)	177.79±22.19 (30.64%)

070

Table E1: Results of significant non-parametric Mann-Whitney and Kruskal-Wallis ranks sum tests as well as Conover-Iman post hoc tests for suspended sediment concentrations (SSC), particulate organic carbon (POC), dissolved organic carbon (DOC), and water isotopic compositions.

Mann-Whitney rank sum test				**Kruskal-Wallis rank sum test**				**Conover-Iman post hoc test**		
		difference	*p*-value		df	H	*p*-value		difference	*p*-value
SSC (mg/L)	baseflow - stormflow	-231.64	**<0.001**	**δ^2H (‰)**	3	25.98	**<0.001**	Fall - Spring	4.23	**<0.001**
								Fall - Summer	-0.81	1.000
POC-F^{14}C	baseflow - stormflow	-0.04	**<0.001**					Spring - Summer	-4.89	**<0.001**
								Fall - Winter	3.86	**0.001**
DOC-F^{14}C	baseflow - stormflow	-0.03	**<0.001**					Spring - Winter	-0.54	1.000
								Summer - Winter	4.56	**<0.001**
				δ^{18}O (‰)	3	24.25	**<0.001**	Fall - Spring	4.29	**<0.001**
								Fall - Summer	-0.74	1.000
								Spring - Summer	-4.88	**<0.001**
								Fall - Winter	3.35	**0.004**
								Spring - Winter	-1.08	0.853
								Summer - Winter	3.99	**<0.001**
				POC-δ^{13}C (‰)	3	24.05	**<0.001**	Fall - Spring	2.73	**0.023**
								Fall - Summer	-3.03	**0.010**
								Spring - Summer	-5.33	**<0.001**
								Fall - Winter	1.15	0.761
								Spring - Winter	-1.67	0.294
								Summer - Winter	4.08	**<0.001**
				DOC-F^{14}C	3	10.55	**0.010**	Fall - Spring	2.20	0.092
								Fall - Summer	3.29	**0.005**
								Spring - Summer	0.91	1.000
								Fall - Winter	1.34	0.556
								Spring - Winter	-0.99	0.970
								Summer - Winter	-2.03	0.139

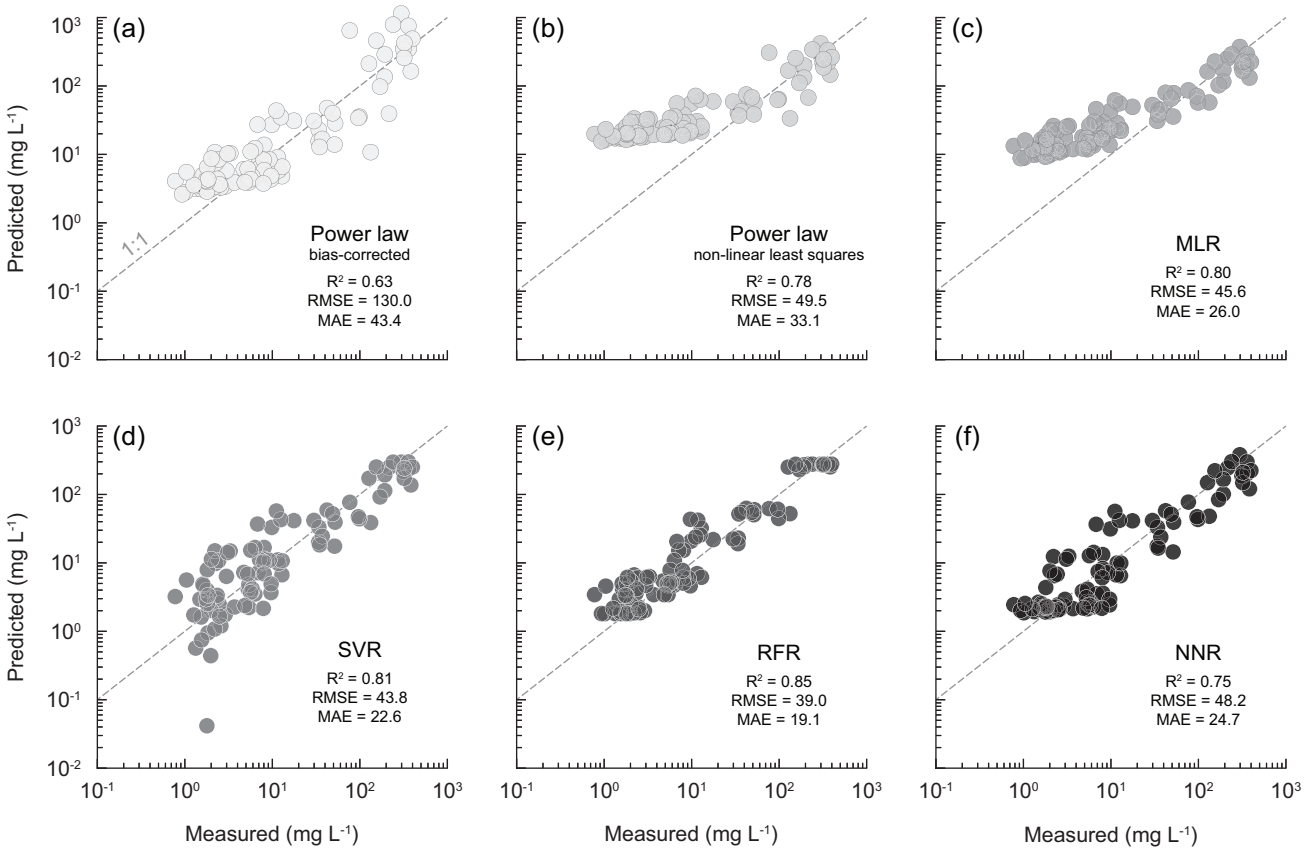

075 **Figure C1:** Performance of (a-b) traditional power law, (c) multiple linear regression (MLR), (d) support vector regression (SVR), (e) random forest regression (RFR), (f) neural network regression (NNR) models. The evaluation is based on observed against predicted suspended sediment concentrations (mg L^{-1}). Performance metrics are based on nested cross-validation (R^2: coefficient of determination, RMSE: root mean squared error, MAE: mean absolute error).

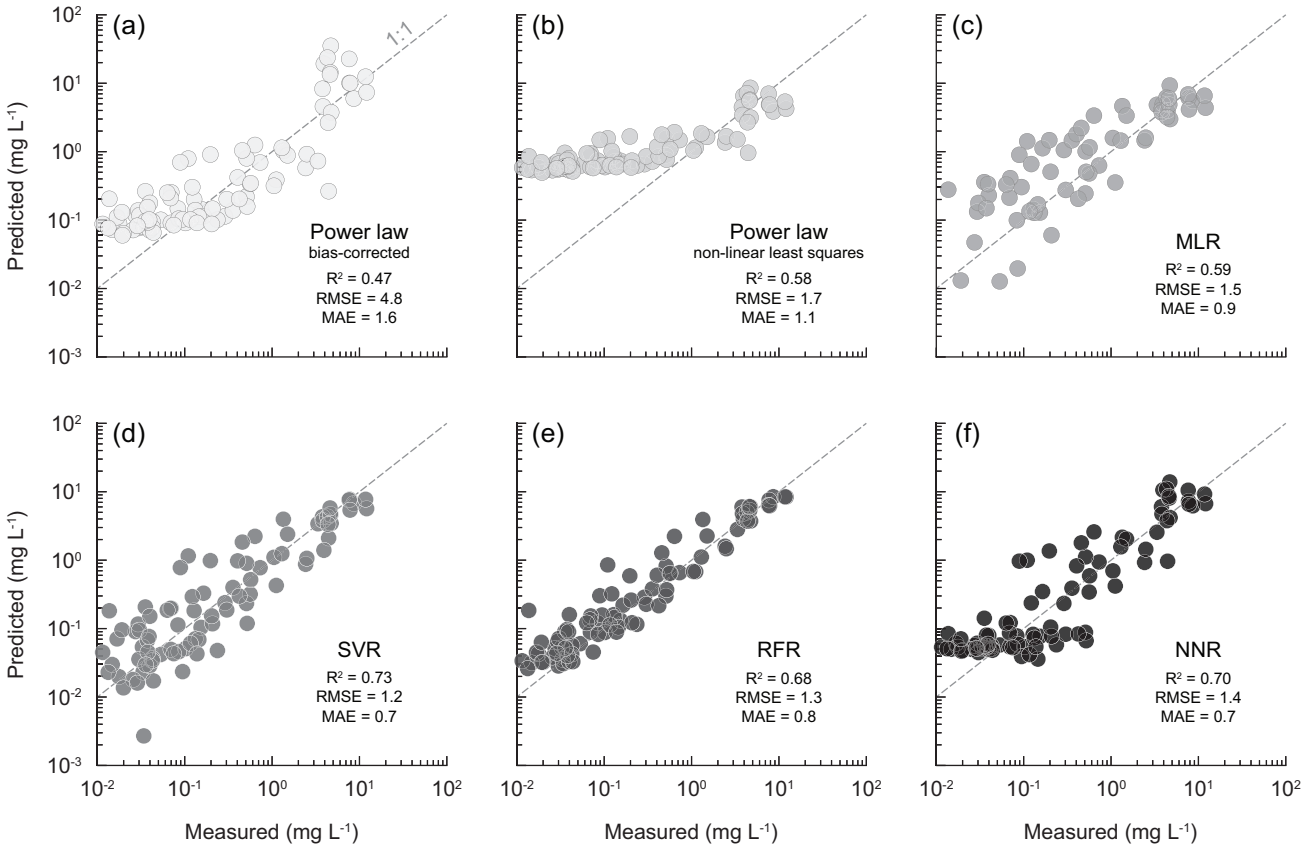

Figure C2: Performance of (a-b) traditional power law, (c) multiple linear regression (MLR), (d) support vector regression (SVR), and (e) random forest regression (RFR), (f) neural network regression (NNR) models. The evaluation is based on observed against predicted particulate organic carbon concentrations (mg L^{-1}). Performance metrics are based on nested cross-validation (R^2: coefficient of determination, RMSE: root mean squared error, MAE: mean absolute error).

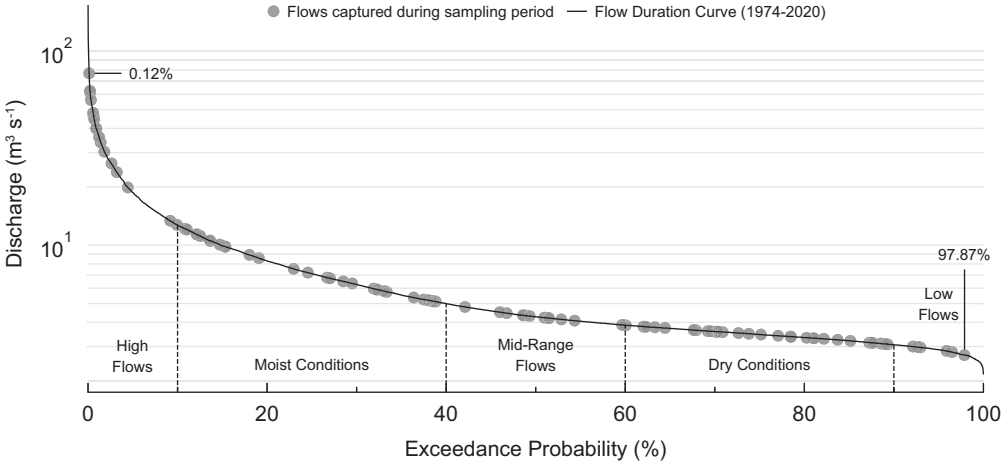

Figure D1: Flow duration curve of the Sihl River spanning from 1974 to 2020. Grey data points indicate sampling points.